〔ウイルス　第62巻　第1号，pp.9-18，2012〕

総　説

2. HTLV-1感染症とmiRNA

山岸　誠，渡邉　俊樹
東京大学大学院新領域創成科学研究科
メディカルゲノム専攻病態医療科学分野

HTLV-1はウイルス遺伝子産物によって感染T細胞を不死化，腫瘍化に導くが，成人T細胞白血病(ATL)を発症するまでの長い潜伏期間の背景にある分子機構は不明な点が多い．感染細胞及びATL細胞において様々な遺伝子発現異常が各々の特徴に寄与しているが，一方でそれらを制御する上流のイベントは不明な点が多かった．miRNAによる遺伝子発現調節という新たな概念が提唱されて以来，HTLV-1/ATLの領域においても複数の研究報告があり，分子レベルでの理解が深まったと言える．特に，ATLの多数の臨床検体を用いた網羅的解析の結果から，腫瘍細胞の特徴の1つであるNF-κBの恒常的活性化の分子メカニズムが明らかとなった．miRNAを介したエピジェネティック制御とNF-κB経路のクロストークも明らかとなり，miRNA研究から新たな分子機構も提唱された．一方でHTLV-1の生活環とmiRNAの関わりやmiRNA発現異常の原因解明など，今後の課題は多い．miRNAは多機能性であり，これらの分子基盤の創設がHTLV-1研究の今後の発展に寄与すると考えられる．

序論

microRNA (miRNA) は19－24merの非コードRNAで，標的遺伝子の3' UTRに結合し，RNAの分解と翻訳阻害を誘導する．標的遺伝子の認識には揺らぎがあるため，一つのmiRNAが複数の遺伝子発現に対して抑制的に働くことができる[1,2,3]．進化的にも保存性が高く，発生や分化，各細胞の機能において不可欠であることは十分に証明されている[1,4,5]．また疾患研究の成果から，miRNAの存在量のバランスが細胞の運命を支配していることも明らかである[6,7,8]．ウイルス学においてもmiRNA研究は盛んに進められており，新たなパラダイムを提供している．それは，外来種であるウイルスは，宿主細胞のmiRNAパターンに影響され，また逆にそのパターンに影響を与えるということである．つまり宿主側はウイルスに対する防御機構としてmiRNAを利用するし，一方でウイルスによるホストmiRNA発現への影響は，ウイルスによる病原性の本質の一つであることも示唆されている[7]．さらに，主にヘルペスウイルスにおいて，ウイルス自身がゲノム上にmiRNAをコードし，自身の生活環の維持と宿主に与える病原性に貢献することも報告されている[7,9,10]．短いRNAがウイルスと宿主の両者に与えるインパクトは，発見当初の予想を遥かに超えるものであったと言えるであろう．

HTLV-1研究領域におけるmiRNA研究は，未だ発展途上であり，十分に理解が進んでいないのが現状である．それは，HTLV-1がウイルス学的手法によって感染実験を進めることが極めて困難であり，HTLV-1とmiRNAの直接的な因果関係を証明することが容易でないことに起因する．しかし，HTLV-1感染によって樹立された細胞株や感染細胞の終末像である成人T細胞白血病（ATL）細胞の詳細な解析が行われ，HTLV-1に関連するmiRNAの全体像はクリアになりつつある．本総説では，HTLV-1/ATL研究領域の成果をまとめ，ウイルスとmiRNAの関係，及びmiRNA異常による分子病態を概説し，miRNA研究の

連絡先
〒108-8639
東京都港区白金台4-6-1
東京大学大学院新領域創成科学研究科
メディカルゲノム専攻病態医療科学分野
TEL: 03-5449-5298
FAX: 03-5449-5418
E-mail: myamagishi@mgs.k.u-tokyo.ac.jp
tnabe@ims.u-tokyo.ac.jp

今後の発展と課題について議論する.

HTLV-1 由来 miRNA の存在について

現在までに，EBV や KSHV などのヘルペスウイルス属を中心に，200 を超える多くのウイルス由来 miRNA が発見されている[7]．これらの DNA ウイルスは，宿主 miRNA と同様にウイルス由来 miRNA を転写から Drosha − Dicer − RISC を経る miRNA の成熟過程をそのまま利用できる．また，ウイルス由来 miRNA は他のウイルスタンパク質と異なり短い RNA であるため免疫原性がなく，ウイルスの複製と潜伏化に適した環境を誘導することができる．さらに少しの変異が及ぼす影響が大きく，二本鎖 DNA の両方を効率よく利用できるという利点も，DNA ウイルスが miRNA をコードする理由であると考えられている．同様の事実はレトロウイルス属にも当てはまることであり，HIV-1 を中心に多くの研究者によって探索が行われている[10,11,12,13]．HTLV-1 についてもウイルス由来 miRNA の存在が期待された．Li らはステムループ構造を予測するアルゴリズムを利用して HTLV-1 のセンス鎖に 3 つ，アンチセンス鎖に 8 つの miRNA を予測している[14]．一方 Lin らは HTLV-1 感染細胞株 MT-2 細胞の 18-24 塩基の RNA から cDNA ライブラリを作成し，698 クローンのシークエンスを行ったが，HTLV-1 由来 miRNA は発見されなかったと報告している[13]．Ruggero らは総説中でさらに詳細に解析したと言及しているが，やはり非常に限定的な検出しかされなかったと述べている[15]．総合すると，HTLV-1 由来 miRNA は存在したとしても，限定された環境下でしかも非常に低レベルであることが想定される．ウイルス由来 miRNA は相補鎖のウイルス RNA に perfect match であり，ウイルスの複製効率とウイルス遺伝子による病原性に強く影響を与える．また多くの宿主遺伝子に対しても影響を及ぼすと考えられる．HTLV-1 が固有の miRNA を発現するか，またそれがどのような機能をもつのかという点は，生理的条件下における詳細な解析により，今後結論が出されるであろう．

HTLV-1 と宿主 miRNA の関係

他のウイルスと同様に，HTLV-1 も RNA として転写される際には複雑な 3' UTR 構造を持ち，宿主及びウイルス由来 miRNA の標的となる条件を満たしている．HIV-1 に関しては複数の研究グループによって宿主 miRNA によるウイルス RNA の抑制と潜伏化誘導が報告されている[16,17,18]．この時，HIV-1 RNA は APOBEC3G とともに，P-body に存在することが示されている[18]．一方 HTLV-1 については，アルゴリズムを用いた標的予測では複数の宿主 miRNA が HTLV-1 RNA に結合できることが予測されているが[15,19]，実験的な検証は行われていない．今後，これらの miRNA 群の発現量とウイルスの複製レベルの関係を調べることにより明らかになるであろう．また，後述する網羅的な miRNA 発現解析の結果と統合することにより，有益な情報が得られると期待される．

一方，HTLV-1 が miRNA の合成経路に対して与える影響については少しずつ理解が進んでいる．Lin らは，宿主の持つ siRNA による標的遺伝子のノックダウン機構に対して，HTLV-1 Tax は大きな影響を与えなかったことから，Tax は RNAi の機構とはリンクしないとしている[13]．一方 Abe らは，HTLV-1 Rex が Dicer と結合し，shRNA から siRNA への成熟過程に影響を与えることを報告している[20]．またつい最近，Rahman らは Jurkat 細胞に Tax を導入した際の miRNA の発現パターンを網羅的に解析した[21]．Tax を導入した細胞では 2 倍以上変化した 41 種の miRNA のうち，35 種の miRNA が減少していた．Tax が miRNA 合成経路に対してどのような分子機構で影響を与えるのか興味深い．また HTLV-1 は主に Tax を介して感染細胞のシグナル伝達系を撹乱することにより[22,23]，miRNA の発現パターンにも大きく影響を与えると考えられる．miRNA の個別の機能が少しずつ明らかとなってきており，改めて HTLV-1 が宿主 miRNA に与える影響の解析が求められている．

HTLV-1 感染細胞における遺伝子発現異常と miRNA

標的遺伝子発現の恒常性の維持が miRNA の本来の機能の一つと言えるが，HTLV-1 感染細胞や ATL 腫瘍細胞では，その恒常性の破綻が明らかに証明されている．Cyclin-CDK 経路，p53 経路，JAK-STAT 経路などの異常の他に，特に NF-κB シグナルの著しい活性化が特徴的である[22,24]．HTLV-1 感染細胞においてはウイルス遺伝子産物である Tax が NF-κB の定型的(canonical)及び非定型的(noncanonical)経路を強烈に活性化し，その結果，感染細胞はアポトーシス抵抗性を獲得する[22,23,25,26]．一方で，ATL 細胞においては Tax の発現は非常に限定的であり，代わりに NF-κB の非定型的経路の上流に位置する NF-κB inducing kinase (NIK) が ATL 細胞において過剰に発現し，恒常的な NF-κB 経路の活性化を誘導する[27]．現在までに様々な NF-κB 経路の阻害剤が開発され，いずれも感染細胞や ATL 細胞に対して強力なアポトーシスを誘導することから，感染細胞及び ATL 細胞は NF-κB 経路に "addict" した状態であると考えられる[28,29,30,31,32,33,34,35]．また興味深い事に，HTLV-1 感染キャリアから分離した末梢血単核球 (PBMC) からは，通常 Tax の発現が認められないが，やはり NF-κB 経路が活性化しているデータが示された[28]．このことからも NF-κB 経路の活性化は HTLV-1 感染症に対する重要な分子標的であると言える．NIK は ATL だけでなく，多発性骨髄腫やびまん性大細胞型 B 細胞リンパ腫 (DLBCL) などの造血器系腫瘍や，乳がんなどの固形がんにおいても重要な分子標的である[36,37,38,39]．NIK の発現レベルは正常

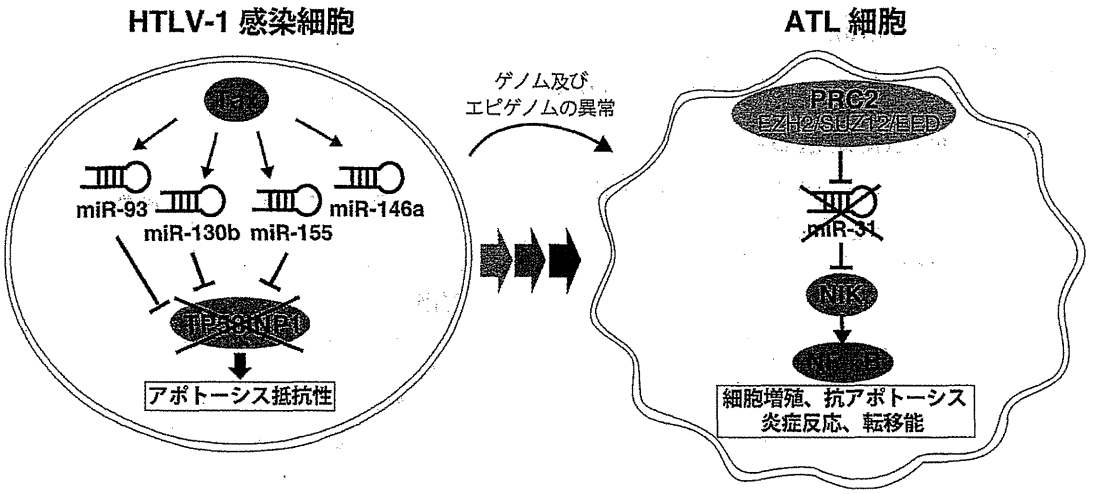

図1　HTLV-1 感染細胞と ATL 細胞における miRNA の異常
感染細胞では Tax によって複数の miRNA が発現誘導され，共通の標的遺伝子である TP53INP1 の発現が減少し，その結果アポトーシス抵抗性が獲得される．一方で ATL 細胞では，ゲノム及びエピゲノム異常の蓄積によって miR-31 の発現が例外なく欠損し，NIK の発現を介した NF-κB 経路の恒常的活性化が誘導される．

細胞では主にタンパク質レベルで制御されているが[40]，ATL 細胞における NIK mRNA の上昇や，他のがんにおける NIK 依存的な NF-κB 経路の活性化メカニズムは明らかになっていなかった．

HTLV-1 の感染が宿主の miRNA パターンに与える直接的な影響は，正確に評価する実験系に高いハードルがある．HIV-1 のように簡便で正確な感染実験系を構築するのが困難であり，また HTLV-1 感染個体からリンパ球のごく一部に相当する感染細胞集団を濃縮する系も確立されていない．従って HTLV-1 感染によって樹立された細胞株による評価が行われている．

Pichler らは，ATL 及び HAM/TSP（HTLV-1 関連脊髄症）患者由来細胞株，HTLV-1 や Tax によってトランスフォームされた細胞株を用いて miRNA の発現レベルを検討した[41]．検討した miRNA は ATL 細胞の起源とされている制御性 T 細胞において重要な miRNA 群[42]，及び当時明らかにされていたがん関連 miRNA 群に限定している．その結果，HTLV-1 関連細胞株で miR-21，miR-24，miR-146a，miR-155 が発現上昇し，miR-223 が発現減少していることを明らかにした．またそのうち miR-146a の過剰発現は Tax による NF-κB 経路の活性化が原因であることも明らかにしている．miR-146a は EBV の LMP1 による NF-κB 経路の活性化によっても誘導されることが報告されている[43,44]．

Yeung らは，7 種類の HTLV-1 関連細胞株と 4 例の急性型 ATL 細胞を用いて 327 種の miRNA の網羅的解析を行った[45]．対照群には正常の PBMC を用いている．彼らはさらに PMA によって PBMC を活性化させた際に上昇する miRNA 群で絞り込みを行い，HTLV-1 感染と T 細胞の活性化によって上昇する miRNA として miR-18a，miR-93，miR-130b を報告している．そのうち，miR-93 と miR-130b の共通する標的遺伝子として TP53INP1 を見いだし，HTLV-1 感染細胞において，miR-93 及び miR-130b の過剰発現が TP53INP1 の発現を低下させることにより，細胞生存の獲得に寄与していることを明らかにした．Pichler らが報告した miR-155 は Yeung らの ATL 細胞における過剰発現 miRNA のリストにも含まれているが，実はその一年前に miR-155 が同じく TP53INP1 を標的とすることが膵臓がんの研究から報告されている[46]．TP53INP1 は様々な固形がんで癌抑制因子として注目されている[47,48,49,50]．また KSHV が発現する miR-K12-11 が miR-155 と高いホモロジーを持ち，miR-155 の過剰発現と同様に B 細胞の増殖をミミックするという興味深い報告もある[51]．HTLV-1 感染細胞においては，複数の miRNA で制御される TP53INP1 の発現低下が重要な役割を持つものと考えられる（**図 1**）．miR-155 の発現は B 細胞株においては LPS によって，前駆脂肪細胞においては TNF-α によって，それぞれ NF-κB 依存的に発現が誘導されることが報告されている[52,53]．また miR-130b のプロモーターにも NF-κB 結合配列があり，上記の miR-146a と同様に，Tax によって miR-130b の発現が誘導される[45]．

ATL における miRNA 異常

Yeung らは 4 例の臨床検体を用いることで ATL 腫瘍細胞における miRNA についても検討している[45]．また 2010 年に Bellon らは，同様に 7 例の ATL 検体について 3 例の正常 PBMC もしくは CD4+ T 細胞と比較を行っている[54]．その結果 ATL では miR-150，miR-155，miR-223，miR-142-3p，miR-142-5p が上昇し，miR-181a，miR-132，

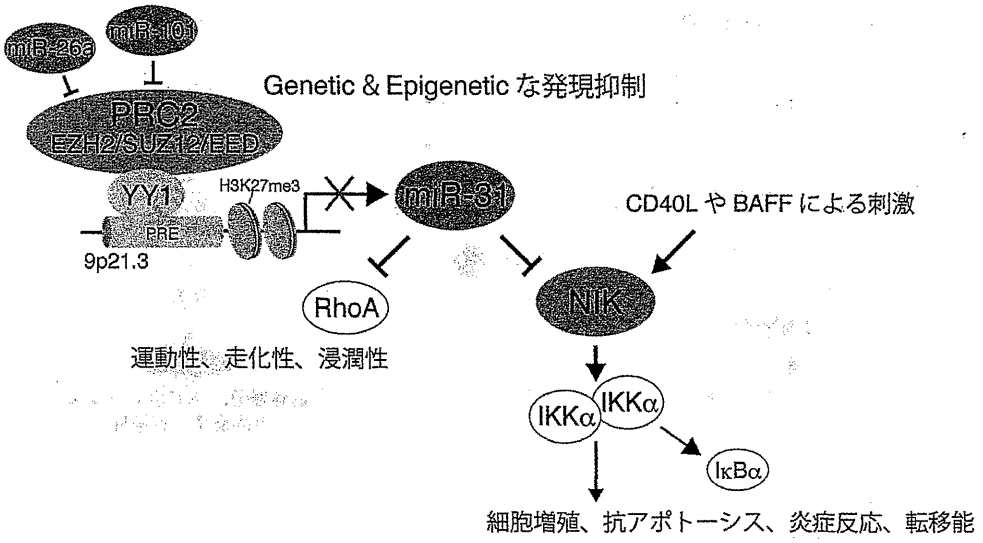

図2 ATL 細胞における miR-31 を取り巻く分子メカニズム
Polycomb 依存的な miR-31 の発現低下は NIK などの標的遺伝子を介して細胞の表現型に影響する．この分子間の関係は様々な細胞種で保存されており，各因子の存在量のバランスによって均衡が保たれている．バランスを崩した細胞は悪性化をたどると考えられる．

miR-125a，miR-146b が減少していると報告している．miR-155 の発現上昇は Pichler ら，Yeung らの報告と一致している．また興味深いことに，Yeung らと Bellon らはそれぞれ，患者由来 ATL 細胞と HTLV-1 によって樹立された細胞株は異なる miRNA 発現パターンを示すと言及している．

上記の3つの報告[41,45,54]では異常を示す miRNA パターンが多様であり，統一したデータが得られていない．その原因は，解析する症例数が少なく，異常を示す miRNA の絞り込みが甘いことが原因であると考えられる．また最近の知見から，リンパ球の各サブセットで miRNA の発現パターンが大きく異なることもわかっており[55,56]，ATL 細胞に対する正確な比較対象（=CD4+ T 細胞）を用意することが，ATL 細胞の異常を正確につかむことにつながると考えられる．また臨床検体については，腫瘍細胞集団と正常細胞の割合も結果に大きく影響するポイントである．

最近我々は，以上の問題に対して回答を得た．我々は HTLV-1 感染者コホート共同研究班 JSPFAD（http://www.htlv1.org/）の全面的協力を得て，世界で初めて ATL 患者由来腫瘍細胞の DNA, mRNA, miRNA の大規模な統合解析を完了した[57]．miRNA 解析のサンプルにはプロウイルス量の多い（＝腫瘍細胞の割合が高い）40 例の ATL 患者由来細胞を用い，さらにコントロール群には ATL 群と年齢を一致させた健常人 CD4+ T 細胞 22 例を用いた．アジレント社の 723 種のヒト miRNA と 76 種のウイルス由来 miRNA を網羅した microarray を用い，非常に厳しい検定をかけて異常 miRNA を割り出した結果，それまでに報告されていた上記の miRNA パターンと異なり，ATL では 61 種の異常 miRNA のうち 59 種の miRNA が正常 T 細胞に比べて著しく低値を示すことがわかった．これは，腫瘍細胞は miRNA の発現が低下傾向にあるという他のがん研究の結果と一致している[58,59]．減少している miRNA リストには，すでに癌抑制性 miRNA として報告されている Let-7 ファミリー[60]や miR-101[61]なども含まれていた．これらの 61 種の miRNA は ATL 細胞の新たな分子マーカーであり，また一つひとつが機能的に腫瘍細胞の特徴に寄与していると考えられる．我々のデータにおいても，上記の先の3つのグループによって報告されている miR-155 の発現上昇が示されていたが，厳しい統計的有意差（$p<0.00001$）は見られなかったため，リストから除外している（筆者ら，unpublished data）．

miR-31 の機能と発現欠損の分子メカニズム

ATL 細胞で見つかった 61 種の発現異常 miRNA のうち，miR-31 が例外なくすべての ATL 患者で減少し，且つ減少のレベルが著しいことに気がついた（0.00403 倍，$p = 2.85 \times 10^{-25}$）．miR-31 の発現減少は，乳がんにおける転移，浸潤過程において重要であることが報告されている[62,63]．我々は，miR-31 の著しい減少が ATL 細胞の特徴を反映していると考え，ATL 細胞の mRNA 発現プロファイルの結果と統合し，さらに *in vitro* の複数の実験を経て，miR-31 の新規標的遺伝子として，ATL 細胞における NF-κB 活性化の原因遺伝子である NIK を見いだした．実験の結果，正常 T 細胞では miR-31 の発現が比較的高く NIK の発現

miRNA	標的遺伝子	参考文献
HTLV-1 感染細胞株		
上昇		
miR-155	TP53INP1	41,54
減少		
miR-150		45,54
miR-223		41,45,54
ATL 細胞		
上昇		
miR-150		45,54
miR-155	TP53INP1	45,54
減少		
miR-31	NIK, RhoA	45,57
miR-125a		54,57
miR-126		45,57
miR-130a		45,57
miR-146b		54,57
miR-181a		54,57
miR-355		45,57

図3 HTLV-1/ATL における miRNA 発現異常
HTLV-1 及び ATL 関連領域の研究のうち，複数の論文で報告されているものを示した．掲載した標的遺伝子は，それらの報告の中で実験的に検証されている遺伝子のみを示している．

を抑制しているが，miR-31 の異常な発現低下が NIK の発現誘導とそれに伴う NF-κB 経路の恒常的活性化を誘発することがわかった（**図1**）．さらに ATL 細胞株及び新鮮 ATL 細胞に対して miR-31 を再導入すると細胞死が誘導された[57]．このことは，miR-31 の細胞内レベルが腫瘍細胞の表現型に直接影響していることを意味し，新しい分子標的としての有用性が示された．

ATL 臨床検体を詳細に解析した結果，miR-31 の発現欠失はゲノムの欠損と Polycomb ファミリー依存的なエピジェネティックな異常によって，すべての ATL 患者で起こっていることがわかった．さらに，Polycomb ファミリーが miR-31 を抑制することによって NIK – NF-κB 経路を活性化する分子機構は，ATL だけでなく乳がん細胞や B 細胞における免疫応答反応においても保存されていることを明らかにした[57,64]．Polycomb ファミリー，NF-κB 経路，miR-31 はそれぞれが単独で多彩な機能を有しており[65,66,67,68,69,70,71,72,73]，細胞の恒常性や分化などの様々な機能に必須であると同時に，さらにクロストークを形成することによって，より複雑な遺伝子発現制御ネットワークに昇華させていると考えられる（**図2**）．我々の実験結果は，ATL 細胞はこの分子ネットワークに依存していることを示しており，エピジェネティックの制御，もしくは miR-31 の補充による新たな治療法の開発につながると期待される．

今後の展望

複数の研究グループによって詳細に解析され[41,45,54,57]，HTLV-1 感染細胞及び ATL 腫瘍細胞の miRNA 発現パターンはほぼ明らかになった（**図3**）．しかし，実際に異常 miRNA の機能とその影響を詳しく解析されているのは miR-93，miR-130b，miR-155 及び miR-31 だけである．標的遺伝子として明らかになった TP53INP1 や NIK にとどまらず，個々の miRNA とその標的遺伝子が感染細胞や腫瘍細胞に対してどのような役割を持つかが，今後の研究課題である．miRNA の標的遺伝子は複数のアルゴリズムによって予測可能であるが，物理的な抑制効果の検証と，標的遺伝子側の機能や挙動も重要な指標となり，従って多角的な実験的検証が必須となることを特筆しておく．

一方で，HTLV-1 と miRNA の研究はまだ始まったばかりである．残っている疑問点は以下に挙げられる．① HTLV-1 が宿主 miRNA システムに与える影響について．感染によって樹立された細胞株からの情報だけでなく，感染というイベントが宿主 miRNA に与えるインパクトについて詳細に検討する必要がある．特に Tax，Rex，HBZ などのウイルス因子が miRNA の合成経路に対してどのような影響を与えるのかは今後の課題である．Rahman らが報告した Tax による宿主 miRNA に対する全体的な抑制効果

は[21]，我々が明らかにしたATLにおけるmiRNAの全体的な減少[57]とリンクするのか，今後の展開が待たれる．②HTLV-1 RNAが宿主もしくはHTLV-1由来miRNAの標的となるのか，実験的検証が必要である．近年になってHTLV-1の伝播様式やレセプターが少しずつ明らかとなっており[74,75,76,77]，またHTLV-1やTaxによる病原性がin vivoにおいても様々なステージにおいて証明され始めている[78,79,80]．様々な環境下におけるHTLV-1の生活環に対してmiRNAがどのような影響を与えるのか，重要な研究課題である．③HTLV-1由来miRNAの存在について．上述したように，ヘルペスウイルスのような高発現miRNAはHTLV-1には存在しないと考えられるが，次世代シークエンサ等の技術導入により明らかにされると期待される．④HTLV-1感染細胞からATL細胞のmiRNAパターンの変遷について．感染細胞はTaxによるNF-κB経路の活性化が良く反映されている一方[45]，終末像であるATLのmiRNAの発現異常は非常に特徴的であり，ゲノム及びエピゲノムの異常によって誘導されるmiRNAパターンにaddictしていると考えられる[57]．どのような分子機構でATL細胞が形成されていくか，エピジェネティックやmiRNA合成経路の詳細な解析が必要である．⑤HTLV-1に関連する他の疾患とmiRNAについて．HAM/TSPやHTLV-1関連ぶどう膜炎（HU）などの疾患についてはmiRNAの検討は行われていない．各疾患の分子病態を理解する上でmiRNAの網羅的な検討は必須である．また感染キャリアにおけるmiRNAパターンを把握することで，発症の分子メカニズムの一端が明らかにされるであろう．

おわりに

1993年に線虫で初めてmiRNAが発見されて以来[81,82]，急速に研究が進展し，miRNAに関する知識も深まってきた．miRNAは遺伝子発現全体を制御する上流の分子群であり，ウイルス感染症を考える上でも欠かす事のできない因子として位置づけられている．ウイルス学のように生理学的意義を検討する学問においては，予測や他の報告だけに頼らず，実験的検証が正しい情報発信に重要である．HTLV-1感染症の分子レベルの理解と治療法の開発を目指す上で，miRNA研究の推進は急務であると考えられる．

参考文献

1）Bartel DP.: MicroRNAs: target recognition and regulatory functions. Cell 136: 215–233, 2009.
2）Cullen BR.: Transcription and processing of human microRNA precursors. Mol. Cell 16: 861–865, 2004.
3）Friedman RC, Farh KK, Burge CB, Bartel DP.: Most mammalian mRNAs are conserved targets of microRNAs. Genome Res. 19: 92–105, 2009.
4）Xiao C, Rajewsky K.: MicroRNA control in the immune system: basic principles. Cell 136: 26–36, 2009.
5）Gangaraju VK, Lin H.: MicroRNAs: key regulators of stem cells. Nat. Rev. Mol. Cell Biol. 10: 116–125, 2009.
6）Ventura A, Jacks T.: MicroRNAs and cancer: short RNAs go a long way. Cell 136: 586–591, 2009.
7）Skalsky RL, Cullen BR.: Viruses, microRNAs, and host interactions. Annu. Rev. Microbiol. 64: 123–141, 2010.
8）Lujambio A, Lowe SW.: The microcosmos of cancer. Nature 482: 347–355, 2012.
9）Pfeffer S, Zavolan M, Grässer FA, Chien M, Russo JJ, Ju J, John B, Enright AJ, Marks D, Sander C, Tuschl T.: Identification of virus-encoded microRNAs. Science 304: 734–736, 2004.
10）Pfeffer S, Sewer A, Lagos-Quintana M, Sheridan R, Sander C, Grässer FA, van Dyk LF, Ho CK, Shuman S, Chien M, Russo JJ, Ju J, Randall G, Lindenbach BD, Rice CM, Simon V, Ho DD, Zavolan M, Tuschl T.: Identification of microRNAs of the herpesvirus family. Nat. Methods 2: 269–276, 2005.
11）Omoto S, Ito M, Tsutsumi Y, Ichikawa Y, Okuyama H, Brisibe EA, Saksena NK, Fujii YR.: HIV-1 nef suppression by virally encoded microRNA. Retrovirology 1: 44, 2004
12）Bennasser Y, Le SY, Benkirane M, Jeang KT.: Evidence that HIV-1 encodes an siRNA and a suppressor of RNA silencing. Immunity 22: 607–619, 2005.
13）Lin J, Cullen BR.: Analysis of the interaction of primate retroviruses with the human RNA interference machinery. J. Virol. 81: 12218–12226, 2007.
14）Li SC, Shiau CK, Lin WC.: Vir-Mir db: prediction of viral microRNA candidate hairpins. Nucleic Acids Res. 36: D184–D189, 2008.
15）Ruggero K, Corradin A, Zanovello P, Amadori A, Bronte V, Ciminale V, D'Agostino DM.: Role of microRNAs in HTLV-1 infection and transformation. Mol. Aspects Med. 31: 367–382, 2010.
16）Huang J, Wang F, Argyris E, Chen K, Liang Z, Tian H, Huang W, Squires K, Verlinghieri G, Zhang H.: Cellular microRNAs contribute to HIV-1 latency in resting primary CD4+ T lymphocytes. Nat. Med. 13: 1241–1247, 2007.
17）Wang X, Ye L, Hou W, Zhou Y, Wang YJ, Metzger DS, Ho WZ.: Cellular microRNA expression correlates with susceptibility of monocytes/macrophages to HIV-1 infection. Blood 113: 671–674, 2009.
18）Nathans R, Chu CY, Serquina AK, Lu CC, Cao H, Rana TM.: Cellular microRNA and P bodies modulate host-HIV-1 interactions. Mol. Cell 34: 696–709, 2009.
19）Hakim ST, Alsayari M, McLean DC, Saleem S, Addanki KC, Aggarwal M, Mahalingam K, Bagasra O.: A large number of the human microRNAs target lentiviruses, retroviruses, and endogenous retroviruses. Biochem. Biophys. Res. Commun. 369: 357–362, 2008.
20）Abe M, Suzuki H, Nishitsuji H, Shida H, Takaku H. Interaction of human T-cell lymphotropic virus type I Rex protein with Dicer suppresses RNAi silencing. FEBS Lett. 584: 4313–4318, 2010.
21）Rahman S, Quann K, Pandya D, Singh S, Khan ZK, Jain P.: HTLV-1 Tax Mediated Downregulation of miR-

NAs Associated with Chromatin Remodeling Factors in T Cells with Stably Integrated Viral Promoter. PLoS One 7: e34490, 2012.
22) Hall WW, Fujii M.: Deregulation of cell-signaling pathways in HTLV-1 infection. Oncogene 24: 5965–5975, 2005.
23) Boxus M, Twizere JC, Legros S, Dewulf JF, Kettmann R, Willems L.: The HTLV-1 Tax interactome. Retrovirology 5: 76, 2008.
24) Matsuoka M, Jeang KT.: Human T-cell leukaemia virus type 1 (HTLV-1) infectivity and cellular transformation. Nat. Rev. Cancer 7: 270–280, 2007.
25) Ruben S, Poteat H, Tan TH, Kawakami K, Roeder R, Haseltine W, Rosen CA.: Cellular transcription factors and regulation of IL-2 receptor gene expression by HTLV-I tax gene product. Science 241: 89–92, 1988.
26) Yoshida M.: Multiple viral strategies of HTLV-1 for dysregulation of cell growth control. Annu. Rev. Immunol. 19: 475–496, 2001.
27) Saitoh Y, Yamamoto N, Dewan MZ, Sugimoto H, Martinez Bruyn VJ, Iwasaki Y, Matsubara K, Qi X, Saitoh T, Imoto I, Inazawa J, Utsunomiya A, Watanabe T, Masuda T, Yamamoto N, Yamaoka S.: Overexpressed NF-kappaB-inducing kinase contributes to the tumorigenesis of adult T-cell leukemia and Hodgkin Reed-Sternberg cells. Blood 111: 5118–5129, 2008.
28) Watanabe M, Ohsugi T, Shoda M, Ishida T, Aizawa S, Maruyama-Nagai M, Utsunomiya A, Koga S, Yamada Y, Kamihira S, Okayama A, Kikuchi H, Uozumi K, Yamaguchi K, Higashihara M, Umezawa K, Watanabe T, Horie R.: Dual targeting of transformed and untransformed HTLV-1-infected T cells by DHMEQ, a potent and selective inhibitor of NF-kappaB, as a strategy for chemoprevention and therapy of adult T-cell leukemia. Blood 106: 2462–2471, 2005.
29) Dewan MZ, Terashima K, Taruishi M, Hasegawa H, Ito M, Tanaka Y, Mori N, Sata T, Koyanagi Y, Maeda M, Kubuki Y, Okayama A, Fujii M, Yamamoto N.: Rapid tumor formation of human T-cell leukemia virus type 1-infected cell lines in novel NOD-SCID/gammac(null) mice: suppression by an inhibitor against NF-kappaB. J. Virol. 77: 5286–5294, 2003.
30) Satou Y, Nosaka K, Koya Y, Yasunaga JI, Toyokuni S, Matsuoka M.: Proteasome inhibitor, bortezomib, potently inhibits the growth of adult T-cell leukemia cells both in vivo and in vitro. Leukemia 18: 1357–1363, 2004.
31) Ohsugi T, Kumasaka T, Ishida A, Ishida T, Horie R, Watanabe T, Umezawa K, Yamaguchi K.: In vitro and in vivo antitumor activity of the NF-kappaB inhibitor DHMEQ in the human T-cell leukemia virus type I-infected cell line, HUT-102. Leuk. Res. 30: 90–97, 2006.
32) Horie R, Watanabe T, Umezawa K.: Blocking NF-kappaB as a potential strategy to treat adult T-cell leukemia/lymphoma. Drug News Perspect. 19: 201–209, 2006.
33) Sanda T, Asamitsu K, Ogura H, Iida S, Utsunomiya A, Ueda R, Okamoto T.: Induction of cell death in adult T-cell leukemia cells by a novel IkappaB kinase inhibitor. Leukemia 20: 590–598, 2006.
34) Nishioka C, Ikezoe T, Yang J, Koeffler HP, Taguchi H.: Fludarabine induces apoptosis of human T-cell leukemia virus type 1-infected T cells via inhibition of the nuclear factor-kappaB signal pathway. Leukemia 21: 1044–1049, 2007.
35) Uota S, Zahidunnabi Dewan M, Saitoh Y, Muto S, Itai A, Utsunomiya A, Watanabe T, Yamamoto N, Yamaoka S.: An IκB kinase 2 inhibitor IMD-0354 suppresses the survival of adult T-cell leukemia cells. Cancer Sci. 103: 100–106, 2012.
36) Annunziata CM, Davis RE, Demchenko Y, Bellamy W, Gabrea A, Zhan F, Lenz G, Hanamura I, Wright G, Xiao W, Dave S, Hurt EM, Tan B, Zhao H, Stephens O, Santra M, Williams DR, Dang L, Barlogie B, Shaughnessy Kuehl WM, Staudt LM.: Frequent engagement of the classical and alternative NF-kappaB pathways by diverse genetic abnormalities in multiple myeloma. Cancer Cell 12: 115–130, 2007.
37) Pham LV, Fu L, Tamayo AT, Bueso-Ramos C, Drakos E, Vega F, Medeiros LJ, Ford RJ.: Constitutive BR3 receptor signaling in diffuse, large B-cell lymphomas stabilizes nuclear factor- κB-inducing kinase while activating both canonical and alternative nuclear factor- κB pathways. Blood 117: 200–210, 2011.
38) Yamamoto M, Ito T, Shimizu T, Ishida T, Semba K, Watanabe S, Yamaguchi N, Inoue JI.: Epigenetic alteration of the NF-kappaB-inducing kinase (NIK) gene is involved in enhanced NIK expression in basal-like breast cancer. Cancer Sci. 101: 2391–2397, 2010.
39) Thu YM, Su Y, Yang J, Splittgerber R, Na S, Boyd A, Mosse C, Simons C, Richmond A.: NF- κB inducing kinase (NIK) modulates melanoma tumorigenesis by regulating expression of pro-survival factors through the β -catenin pathway. Oncogene: advance online publication, 2011.
40) Sun SC.: Non-canonical NF-κB signaling pathway. Cell Res. 21: 71–85, 2011.
41) Pichler K, Schneider G, Grassmann R.: MicroRNA miR-146a and further oncogenesis-related cellular microRNAs are dysregulated in HTLV-1-transformed T lymphocytes. Retrovirology 5: 100, 2008.
42) Cobb BS, Hertweck A, Smith J, O'Connor E, Graf D, Cook T, Smale ST, Sakaguchi S, Livesey FJ, Fisher AG, Merkenschlager M.: A role for Dicer in immune regulation. J. Exp. Med. 203: 2519–2527, 2006.
43) Motsch N, Pfuhl T, Mrazek J, Barth S, Grässer FA.: Epstein-Barr virus-encoded latent membrane protein 1 (LMP1) induces the expression of the cellular microRNA miR-146a. RNA Biol. 4: 131–137, 2007.
44) Cameron JE, Yin Q, Fewell C, Lacey M, McBride J, Wang X, Lin Z, Schaefer BC, Flemington EK.: Epstein-Barr virus latent membrane protein 1 induces cellular MicroRNA miR-146a, a modulator of lymphocyte signaling pathways. J. Virol. 82: 1946–1958, 2008.
45) Yeung ML, Yasunaga J, Bennasser Y, Dusetti N, Harris D, Ahmad N, Matsuoka M, Jeang KT.: Roles for microRNAs, miR-93 and miR-130b, and tumor protein

53-induced nuclear protein 1 tumor suppressor in cell growth dysregulation by human T-cell lymphotrophic virus 1. Cancer Res. 68: 8976–8985, 2008.
46) Gironella M, Seux M, Xie MJ, Cano C, Tomasini R, Gommeaux J, Garcia S, Nowak J, Yeung ML, Jeang KT, Chaix A, Fazli L, Motoo Y, Wang Q, Rocchi P, Russo A, Gleave M, Dagorn JC, Iovanna JL, Carrier A, Pébusque MJ, Dusetti NJ.: Tumor protein 53-induced nuclear protein 1 expression is repressed by miR-155, and its restoration inhibits pancreatic tumor development. Proc. Natl. Acad. Sci. U S A. 104: 16170–16175, 2007.
47) Gommeaux J, Cano C, Garcia S, Gironella M, Pietri S, Culcasi M, Pébusque MJ, Malissen B, Dusetti N, Iovanna J, Carrier A.: Colitis and colitis-associated cancer are exacerbated in mice deficient for tumor protein 53-induced nuclear protein 1. Mol. Cell. Biol. 27: 2215–2228, 2007.
48) Ito Y, Motoo Y, Yoshida H, Iovanna JL, Takamura Y, Miya A, Kuma K, Miyauchi A.: Decreased expression of tumor protein p53-induced nuclear protein 1 (TP53INP1) in breast carcinoma. Anticancer Res. 26: 4391–4395, 2006.
49) Jiang PH, Motoo Y, Garcia S, Iovanna JL, Pebusque MJ, Sawabu N.: Down-expression of tumor protein p53-induced nuclear protein 1 in human gastric cancer. World J. Gastroenterol. 12: 691–696, 2006.
50) Bonazzi VF, Irwin D, Hayward NK.: Identification of candidate tumor suppressor genes inactivated by promoter methylation in melanoma. Genes Chromosomes Cancer 48: 10–21, 2009.
51) Gottwein E, Mukherjee N, Sachse C, Frenzel C, Majoros WH, Chi JT, Braich R, Manoharan M, Soutschek J, Ohler U, Cullen BR.: A viral microRNA functions as an orthologue of cellular miR-155. Nature 450: 1096–1099, 2007.
52) Thompson RC, Herscovitch M, Zhao I, Ford TJ, Gilmore TD.: NF-kappaB down-regulates expression of the B-lymphoma marker CD10 through a miR-155/PU.1 pathway. J. Biol. Chem. 286: 1675–1682, 2011.
53) Liu S, Yang Y, Wu J.: TNF α -induced up-regulation of miR-155 inhibits adipogenesis by down-regulating early adipogenic transcription factors. Biochem. Biophys. Res. Commun. 414: 618–624, 2011.
54) Bellon M, Lepelletier Y, Hermine O, Nicot C.: Deregulation of microRNA involved in hematopoiesis and the immune response in HTLV-I adult T-cell leukemia. Blood 113: 4914–4917, 2009.
55) Chen CZ, Li L, Lodish HF, Bartel DP.: MicroRNAs modulate hematopoietic lineage differentiation. Science 303: 83–86, 2004.
56) Lu LF, Liston A.: MicroRNA in the immune system, microRNA as an immune system. Immunology 127: 291–298, 2009.
57) Yamagishi M, Nakano K, Miyake A, Yamochi T, Kagami Y, Tsutsumi A, Matsuda Y, Sato-Otsubo A, Muto S, Utsunomiya A, Yamaguchi K, Uchimaru K, Ogawa S, Watanabe T.: Polycomb-Mediated Loss of miR-31 Activates NIK-Dependent NF- κB Pathway in Adult T Cell Leukemia and Other Cancers. Cancer Cell 21: 121–135, 2012.
58) Lu J, Getz G, Miska EA, Alvarez-Saavedra E, Lamb J, Peck D, Sweet-Cordero A, Ebert BL, Mak RH, Ferrando AA, Downing JR, Jacks T, Horvitz HR, Golub TR.: MicroRNA expression profiles classify human cancers. Nature 435: 834–838, 2005.
59) Gaur A, Jewell DA, Liang Y, Ridzon D, Moore JH, Chen C, Ambros VR, Israel MA.: Characterization of microRNA expression levels and their biological correlates in human cancer cell lines. Cancer Res. 67: 2456–2468, 2007.
60) Roush S, Slack FJ.: The let-7 family of microRNAs. Trends Cell Biol. 18: 505–516, 2008.
61) Varambally S, Cao Q, Mani RS, Shankar S, Wang X, Ateeq B, Laxman B, Cao X, Jing X, Ramnarayanan K, Brenner JC, Yu J, Kim JH, Han B, Tan P, Kumar-Sinha C, Lonigro RJ, Palanisamy N, Maher CA, Chinnaiyan AM.: Genomic loss of microRNA-101 leads to overexpression of histone methyltransferase EZH2 in cancer. Science 322: 1695–1699, 2008.
62) Valastyan S, Reinhardt F, Benaich N, Calogrias D, Szász AM, Wang ZC, Brock JE, Richardson AL, Weinberg RA.: A pleiotropically acting microRNA, miR-31, inhibits breast cancer metastasis. Cell 137: 1032–1046, 2009.
63) Valastyan S, Benaich N, Chang A, Reinhardt F, Weinberg RA.: Concomitant suppression of three target genes can explain the impact of a microRNA on metastasis. Genes Dev. 23: 2592–2597, 2009.
64) Uribesalgo I, Ballare C, Croce LD.: Polycomb Regulates NF- κB Signaling in Cancer through miRNA. Cancer Cell 21: 5–7, 2012.
65) Sparmann A, van Lohuizen M.: Polycomb silencers control cell fate, development and cancer. Nat. Rev. Cancer 6: 846–856, 2006.
66) Simon JA, Kingston RE.: Mechanisms of polycomb gene silencing: knowns and unknowns. Nat. Rev. Mol. Cell Biol. 10: 697–708, 2009.
67) Rouas R, Fayyad-Kazan H, El Zein N, Lewalle P, Rothé F, Simion A, Akl H, Mourtada M, El Rifai M, Burny A, Romero P, Martiat P, Badran B.: Human natural Treg microRNA signature: role of microRNA-31 and microRNA-21 in FOXP3 expression. Eur. J. Immunol. 39: 1608–1618, 2009.
68) Liu CJ, Tsai MM, Hung PS, Kao SY, Liu TY, Wu KJ, Chiou SH, Lin SC, Chang KW.: miR-31 Ablates Expression of the HIF Regulatory Factor FIH to Activate the HIF Pathway in Head and Neck Carcinoma. Cancer Res. 70: 1635–1644, 2010.
69) Creighton CJ, Fountain MD, Yu Z, Nagaraja AK, Zhu H, Khan M, Olokpa E, Zariff A, Gunaratne PH, Matzuk MM, Anderson ML.: Molecular Profiling Uncovers a p53-Associated Role for MicroRNA-31 in Inhibiting the Proliferation of Serous Ovarian Carcinomas and Other Cancers. Cancer Res. 70: 1906–1915, 2010.
70) Valastyan S, Weinberg RA.: miR-31: A crucial overseer of tumor metastasis and other emerging roles. Cell Cycle 9: 2124–2129, 2010.
71) Hayden MS, Ghosh S.: Signaling to NF-kappaB. Genes

Dev. 18: 2195–2224, 2004.
72) Bonizzi G, Karin M.: The two NF-kappaB activation pathways and their role in innate and adaptive immunity. Trends Immunol. 25: 280–288, 2004.
73) Hayden MS, Ghosh S.: Shared principles in NF-kappaB signaling. Cell 132: 344–362, 2008.
74) Manel N, Kim FJ, Kinet S, Taylor N, Sitbon M, Battini JL.: The ubiquitous glucose transporter GLUT-1 is a receptor for HTLV. Cell 115: 449–459, 2003.
75) Ghez D, Lepelletier Y, Jones KS, Pique C, Hermine O.: Current concepts regarding the HTLV-1 receptor complex. Retrovirology 7: 99, 2010.
76) Igakura T, Stinchcombe JC, Goon PK, Taylor GP, Weber JN, Griffiths GM, Tanaka Y, Osame M, Bangham CR.: Spread of HTLV-I between lymphocytes by virus-induced polarization of the cytoskeleton. Science 299: 1713–1716, 2003.
77) Pais-Correia AM, Sachse M, Guadagnini S, Robbiati V, Lasserre R, Gessain A, Gout O, Alcover A, Thoulouze MI.: Biofilm-like extracellular viral assemblies mediate HTLV-1 cell-to-cell transmission at virological synapses. Nat. Med. 16: 83–89, 2010.
78) Hasegawa H, Sawa H, Lewis MJ, Orba Y, Sheehy N, Yamamoto Y, Ichinohe T, Tsunetsugu-Yokota Y, Katano H, Takahashi H, Matsuda J, Sata T, Kurata T, Nagashima K, Hall WW.: Thymus-derived leukemia-lymphoma in mice transgenic for the Tax gene of human T-lymphotropic virus type I. Nat. Med. 12: 466–472, 2006.
79) Ohsugi T, Kumasaka T, Okada S, Urano T.: The Tax protein of HTLV-1 promotes oncogenesis in not only immature T cells but also mature T cells. Nat. Med. 13: 527–528, 2007.
80) Banerjee P, Tripp A, Lairmore MD, Crawford L, Sieburg M, Ramos JC, Harrington W Jr, Beilke MA, Feuer G.: Adult T-cell leukemia/lymphoma development in HTLV-1-infected humanized SCID mice. Blood 115: 2640–2648, 2010.
81) Lee RC, Feinbaum RL, Ambros V.: The C. elegans heterochronic gene lin-4 encodes small RNAs with antisense complementarity to lin-14. Cell 75: 843–854, 1993.
82) Wightman B, Ha I, Ruvkun G.: Posttranscriptional regulation of the heterochronic gene lin-14 by lin-4 mediates temporal pattern formation in C. elegans. Cell 75: 855–862, 1993.

Molecular BioSystems

Cite this: *Mol. BioSyst.*, 2012, **8**, 2050–2053

www.rsc.org/molecularbiosystems

COMMUNICATION

Structural and thermodynamic characterization of the self-adhesive properties of human P-cadherin†

Shota Kudo,[a] Jose M. M. Caaveiro,[b] Takamitsu Miyafusa,[a] Shuichiro Goda,[c] Keisuke Ishii,[d] Tadashi Matsuura,[d] Yukio Sudou,[d] Tatsuhiko Kodama,[e] Takao Hamakubo[e] and Kouhei Tsumoto*[ab]

Received 26th April 2012, Accepted 22nd May 2012
DOI: 10.1039/c2mb25161b

Human P-cadherin is a promising therapeutic target against cancer. However, its characterization at the molecular level is still lacking. We report that human P-cadherin associated irreversibly in a distinct dimer configuration. Unexpectedly, the divalent cation Ca^{2+} was not necessary for dimerization, although it greatly stabilized the protein–protein complex.

Cadherins are a large family of cell-surface membrane proteins that mediate intercellular adhesion and maintain solid tissue.[1] Classical cadherins are the largest and best characterized group. They self-associate in a Ca^{2+}-dependent manner during cell–cell adhesion owing to their extracellular cadherin (EC) domains.[2] Dimerization occurs at the N-terminal end by a strand-swap mechanism that involves residues Asp1 and Trp2.

P-cadherin belongs to the classical cadherin family, showing high similarity at the primary sequence level to model proteins E-cadherin and N-cadherin (ESI†, Fig. S1). Human P-cadherin is weakly expressed in the basal layers of stratified epithelia where it regulates tissue maintenance and development, and drives cell proliferation.[1,3] Human P-cadherin is also over-expressed in pancreatic, lung, gastric, and colorectal cancers.[4] Importantly, inhibition of the adhesive properties of P-cadherin by therapeutic antibodies suppresses the growth of primary tumors and their metastatic progression.[5] Although P-cadherin is a promising therapeutic candidate, the protein has not been yet subjected to detailed biochemical and biophysical characterization. To understand the adhesive mechanism of P-cadherin we prepared recombinant forms of the first and second ectodomains (EC12). These two domains constitute the minimum structural element responsible for dimerization in other classical cadherins.[2]

[a] *Department of Medical Genome Sciences, The University of Tokyo, Tokyo, 108-8639, Japan. E-mail: tsumoto@ims.u-tokyo.ac.jp; Fax: +81 3-6409-2129; Tel: +81 3-5449-5316*
[b] *Institute of Medical Sciences, The University of Tokyo, Tokyo, 108-8639, Japan*
[c] *Faculty of Engineering, Nagasaki University, Nagasaki, 852-8521, Japan*
[d] *Perseus Proteomics Inc., Komaba, Tokyo, 153-0041, Japan*
[e] *Research Center for Advanced Science and Technology, The University of Tokyo, Tokyo, 153-8904, Japan*
† Electronic supplementary information (ESI) available: Experimental details; sequence alignment; AF4; SAXS; intrinsic fluorescence. See DOI: 10.1039/c2mb25161b

Cloning, expression, and purification of EC12 (residues 1–241) of the mature human P-cadherin were carried out with a pET-SUMO vector as described in ESI.† After purification and cleavage of the N-terminal SUMO-tag we obtained protein >95% homogeneous as judged by SDS-PAGE (not shown). Molecular size was evaluated by analytical size exclusion chromatography (SEC) and asymmetric flow-field flow-fractionation (AF4) (ESI†). Small-angle X-ray scattering (SAXS) data were collected at beamline BL-10C of the Photon Factory in Tsukuba (Japan) as described previously.[6] Thermodynamic analysis carried out by differential scanning calorimetry (DSC) and isothermal titration calorimetry (ITC) is explained in ESI.†

SEC and AF4 were employed to monitor the dimerization state of EC12 in the presence of Ca^{2+} (Fig. 1A; ESI†, Fig. S2A). The SEC profile showed a single and well-resolved peak centered at 11.2 ml. The position of this peak contrasted with that of the mutein EC12-W2A (12.3 ml), a monomeric variant lacking the key residue Trp2 necessary for the dimerization of cadherins.[7] The molecular weight of EC12 was determined by AF4 because the elongated shape of cadherins prevents accurate determination by SEC. The value obtained by AF4 was 43 kDa, a figure compatible with the predicted size of the dimer (53 kDa).

SAXS further revealed the dimeric nature of P-cadherin in solution (Fig. 1B). We found that the experimental SAXS profile of EC12 and the calculated curve of the strand-swap dimer (ss-dimer) of the highly homologous human E-cadherin (PDB entry code 2O72) superimposed well. The excellent agreement between the experimental and calculated curves contrasted with the poor fitting when the monomeric form of E-cadherin was used (ESI†, Fig. S3). In aggregate, SEC, SAXS, AF4, and mutational analysis demonstrated that P-cadherin self-associates in solution in the ss-dimer configuration in a manner analogous to that of E- and N-cadherins.[7]

Ca^{2+} is a cation intimately linked to the assembly of classical cadherins.[2,8] The first and second EC domains of E- and N-cadherin bind three atoms of Ca^{2+} before triggering protein dimerization, and this cation is also necessary for the maintenance of the dimeric state.[9] To examine the effect of Ca^{2+} on the adhesive properties of P-cadherin we followed two alternative procedures. In the first approach, Ca^{2+} ions were removed prior to the association step (before dimerization). Because the protein is expressed with a 12 kDa His_6-SUMO-tag

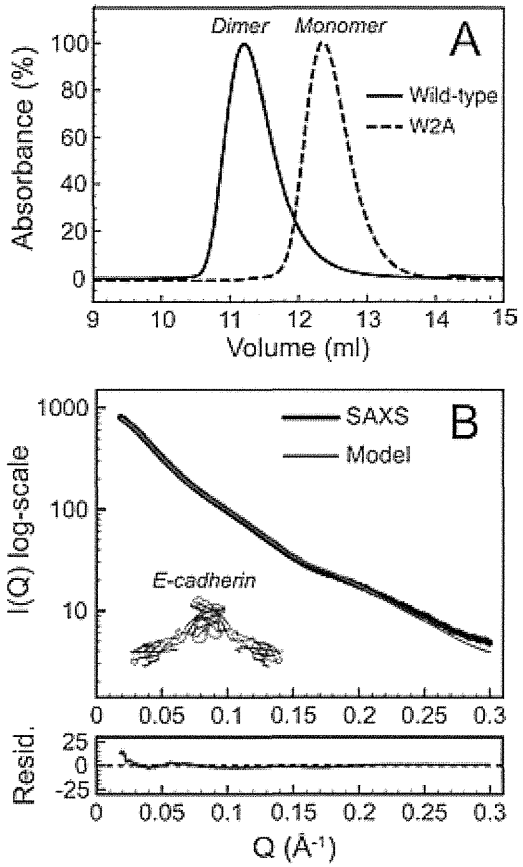

Fig. 1 Dimerization of P-cadherin. (A) SEC profile of wild-type EC12 (solid line) and mutein W2A (broken line). (B) Experimental SAXS profile of P-cadherin EC12 (black) and theoretical curve of crystallographic ss-dimer of E-cadherin (red) calculated with the program FoXS of the Chimera suite (PDB entry code 2O72).[12] Buffer contained 3 mM Ca^{2+}.

at the N-terminal, EC12 remains as a monomer until protease cleavage of the SUMO-tag. This procedure mimicked the activation route of classical cadherins *in vivo*.[2] By incubating the samples with excess EDTA before protease cleavage, we could study the dimerization of EC12 in the absence of Ca^{2+} ions. In the second approach, Ca^{2+} ions were removed with EDTA after the dimerization reaction had proceeded in the presence of Ca^{2+}.

SEC was employed to monitor the self-dimerization of EC12 (Fig. 2). The chromatographic profiles of the two types of Ca^{2+}-depleted samples were essentially identical to each other, and also very similar to that of dimeric EC12 in the presence of Ca^{2+} (see Fig. 1A). We observed a small shoulder corresponding to the monomeric form of the protein. The fraction of the monomeric form estimated from SEC data was very small (<5%). The molecular weight of the major peak determined by AF4 was 53 kDa, a value consistent with the dimeric form of the protein (ESI†, Fig. S2B). The fluorescence spectra of Ca^{2+}-depleted samples indicated that the dimerization site around Trp2 in either structure was essentially identical (ESI†, Fig. S4). Overall, this set of experiments demonstrated that dimerizaton of EC12 was independent of Ca^{2+}. This is an unusual observation in the cadherin family of proteins, and

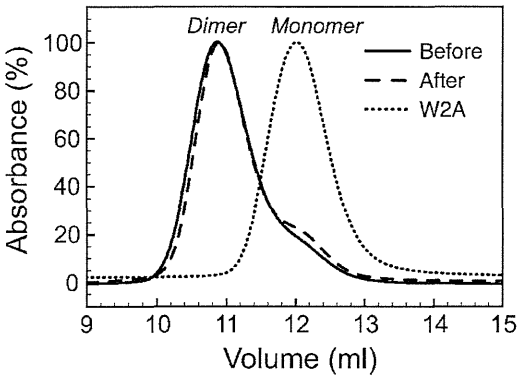

Fig. 2 Dimerization of P-cadherin is largely independent of Ca^{2+}. SEC profiles of samples of EC12 obtained after Ca^{2+}-depletion by two different methodologies: Ca^{2+} was removed before (solid line), or after (broken line) treatment with SUMO protease. Dotted line corresponds to mutein W2A.

suggested that the self-affinity of P-cadherin is higher than that of homologous cadherins.[9]

The thermodynamic basis for the binding of Ca^{2+} to P-cadherin was determined by ITC and DSC (Fig. 3). Titration of apo-EC12 with Ca^{2+} gave rise to a typical sigmoidal binding isotherm (Fig. 3A). Each molecule of apo-EC12 bound an average of 2.7 atoms of Ca^{2+}. This value was consistent with the three Ca^{2+} ions found in the crystal structures of homologous E- and N-cadherins. This result also validated the methodology employed to remove the Ca^{2+} ions from the protein samples. The binding constant (dissociation constant, K_D) obtained from the fitting procedure was 23 ± 6 μM. Binding of Ca^{2+} to P-cadherin was driven by both favourable enthalpy (ΔH_B = –2.6 ± 0.1 kcal mol^{-1}) and entropy terms ($-T\Delta S_B$ = –3.6 kcal mol^{-1}). These results

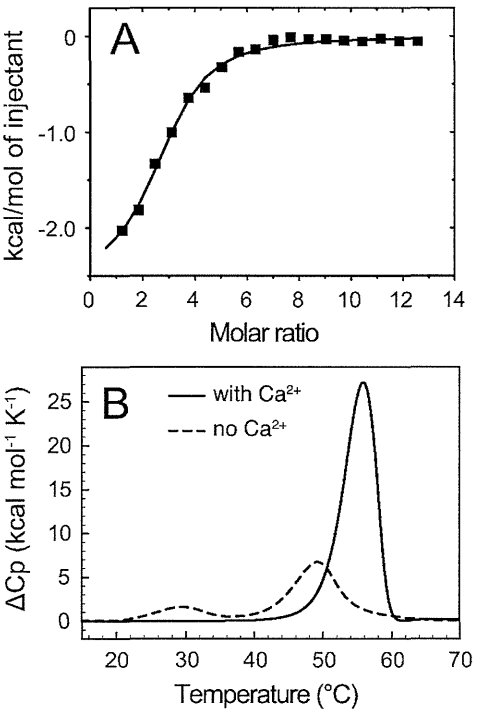

Fig. 3 Thermodynamic analysis. (A) Binding isotherm of Ca^{2+} to apo-EC12. (B) Thermal stability of EC12 in the presence of 3 mM Ca^{2+} (solid line), or Ca^{2+}-depleted samples (broken line).

Table 1 Effect of Ca^{2+} on the stability of P-cadherin

Ca^{2+}	T_{M1} (°C)	ΔH_1 (kcal mol^{-1})	T_{M2} (°C)	ΔH_2 (kcal mol^{-1})
Absent	49.0 ± 0.1	−61 ± 0.3	29.6 ± 0.1	−16 ± 0.5
Present	55.4 ± 0.1	−155 ± 1.0	N.O.[a]	N.O.

[a] N.O., not observed.

revealed a complex thermodynamic pattern that did not fit a simple interaction model.[10] We suggest that binding of Ca^{2+} to P-cadherin involved various sources of stabilization, in addition to the electrostatic interaction between Ca^{2+} and protein.

The thermal denaturation profile of EC12 in the absence of Ca^{2+} also displayed a complex pattern (Fig. 3B and Table 1). First, the thermal transition did not obey the classical two-state equation. Instead, the Ca^{2+}-depleted form of P-cadherin gave rise to two separate transitions of variable enthalpy (it is tempting to speculate that each peak could correspond to the individual transition of each domain). The mid-point transitions occurred at temperatures of 49 and 30 °C, respectively, although only the second transition displayed a significant enthalpy change (ΔH = −61 ± 0.3 kcal mol^{-1}).

In contrast, the presence of Ca^{2+} dramatically altered the thermal profile of EC12. First, the thermogram showed high cooperativity and displayed only one transition. Second, the thermal stability T_M increased by 6 °C when Ca^{2+} was present. And third, the enthalpy of the transition increased significantly under Ca^{2+} conditions (ΔH = −155 kcal mol^{-1}; $\Delta\Delta H$ = −95 kcal mol^{-1}). We note that the magnitude of $\Delta\Delta H$ is almost an order of magnitude higher than that determined in analogous experiments with E- and N-cadherin.[9,11] This analysis thus demonstrated the key role of Ca^{2+} in the thermal stabilization of P-cadherin.

We summarize our results in Fig. 4. P-cadherin can adopt three possible configurations in solution: (i) monomer, (ii) flexible dimeric state, and (iii) stable ss-dimer. The monomeric form of P-cadherin is not favoured thermodynamically, and thus dimerizes spontaneously even in the absence of Ca^{2+}. These observations mark a departure from the behaviour of other members of the classical cadherin family, and suggested stronger self-adhesive properties of P-cadherin. We propose that these novel properties arise from differences at the primary sequence level, in particular in the critical N-terminal region. We also speculate that cell–cell adhesion mediated by human P-cadherin is persistent, which could facilitate the attachment of cancer cells expressing high levels of this protein. We hope these results will guide the exploration of therapeutic treatments based on human P-cadherin.

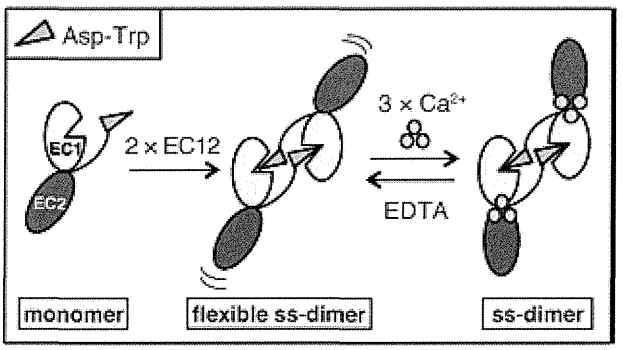

Fig. 4 Model of dimerization of P-cadherin. EC12 self-associates irreversibly in the ss-dimer configuration without the need of Ca^{2+}. This form of the ss-dimer can bind up to three Ca^{2+} ions that greatly stabilize the dimeric configuration.

Conclusions

We found that human P-cadherin self-associates in the ss-dimer configuration, similarly to other classical cadherin proteins. Unexpectedly, Ca^{2+} was not necessary for the dimerization of P-cadherin, although it enhanced its thermal stability. Overall, our analysis suggested that P-cadherin possesses stronger adhesive properties than other members of the classical cadherin family.

Abbreviations

EC	Extracellular cadherin
IMAC	Immobilized-metal affinity chromatography
SEC	Size exclusion chromatography
AF4	Asymmetric flow-field flow-fractionation
DSC	Differential scanning calorimetry
ITC	Isothermal titration calorimetry
SAXS	Small-angle X-ray scattering
ss-dimer	Strand-swap dimer

Acknowledgements

This work was supported by the Funding program for world-leading Innovative R&D on Science and Technology (FIRST) of the Japan Society for the Promotion of Science. Access to beamline BL-10C was granted by the Photon Factory Advisory Committee (Proposal Numbers 2011G573, 2011G145, and 2011G535).

Notes and references

1 M. Takeichi, *Development*, 1988, **102**, 639; M. Takeichi, *Annu. Rev. Biochem.*, 1990, **59**, 237; B. D. Angst, C. Marcozzi and A. I. Magee, *J. Cell Sci.*, 2001, **114**, 629.
2 B. Nagar, M. Overduin, M. Ikura and J. M. Rini, *Nature*, 1996, **380**, 360; D. Haussinger, T. Ahrens, T. Aberle, J. Engel, J. Stetefeld and S. Grzesiek, *EMBO J.*, 2004, **23**, 1699; O. J. Harrison, E. M. Corps and P. J. Kilshaw, *J. Cell Sci.*, 2005, **118**, 4123; O. J. Harrison, F. Bahna, P. S. Katsamba, X. Jin, J. Brasch, J. Vendome, G. Ahlsen, K. J. Carroll, S. R. Price, B. Honig and L. Shapiro, *Nat. Struct. Mol. Biol.*, 2010, **17**, 348.
3 R. T. Bryan and C. Tselepis, *J. Urol.*, 2010, **184**, 423.
4 Y. Shimoyama, S. Hirohashi, S. Hirano, M. Noguchi, Y. Shimosato, M. Takeichi and O. Abe, *Cancer Res.*, 1989, **49**, 2128; K. Imai, S. Hirata, A. Irie, S. Senju, Y. Ikuta, K. Yokomine, M. Harao, M. Inoue, T. Tsunoda, S. Nakatsuru, H. Nakagawa, Y. Nakamura, H. Baba and Y. Nishimura, *Clin. Cancer Res.*, 2008, **14**, 6487.
5 C. C. Zhang, Z. Yan, Q. Zhang, K. Kuszpit, K. Zasadny, M. Qiu, C. L. Painter, A. Wong, E. Kraynov, M. E. Arango, P. P. Mehta, I. Popoff, G. F. Casperson, G. Los, S. Bender, K. Anderes, J. G. Christensen and T. VanArsdale, *Clin. Cancer Res.*, 2010, **16**, 5177; H. Yoshioka, S. Yamamoto, H. Hanaoka, Y. Iida, P. Paudyal, T. Higuchi, H. Tominaga, N. Oriuchi, H. Nakagawa, Y. Shiba, K. Yoshida, R. Osawa, T. Katagiri, T. Tsunoda, Y. Nakamura and K. Endo, *Cancer Immunol. Immunother.*, 2012, DOI: 10.1007/s00262-011-1186-0.
6 Y. Hiragi, Y. Seki, K. Ichimura and K. Soda, *J. Appl. Crystallogr.*, 2002, **35**, 1; T. Ueki, Y. Hiragi, M. Kataoka, Y. Inoko, Y. Amemiya, Y. Izumi, H. Tagawa and Y. Muroga, *Biophys. Chem.*, 1985, **23**, 115.
7 K. Tamura, W.-S. Shan, W. Hendrickson, D. R. Colman and L. Shapiro, *Neuron*, 1998, **20**, 1153; E. Parisini, J. M. Higgins, J. H. Liu, M. B. Brenner and J. H. Wang, *J. Mol. Biol.*, 2007, **373**, 401.

8 C. Ciatto, F. Bahna, N. Zampieri, H. C. VanSteenhouse, P. S. Katsamba, G. Ahlsen, O. J. Harrison, J. Brasch, X. Jin, S. Posy, J. Vendome, B. Ranscht, T. M. Jessell, B. Honig and L. Shapiro, *Nat. Struct. Mol. Biol.*, 2010, **17**, 339; N. Vunnam and S. Pedigo, *Biochemistry*, 2011, **50**, 2973.
9 N. Vunnam, J. Flint, A. Balbo, P. Schuck and S. Pedigo, *Biochemistry*, 2011, **50**, 2951.
10 P. D. Ross and S. Subramanian, *Biochemistry*, 1981, **20**, 3096.
11 N. Vunnam and S. Pedigo, *Biochemistry*, 2011, **50**, 8437; N. Vunnam and S. Pedigo, *Biochemistry*, 2011, **50**, 6959.
12 D. Schneidman-Duhovny, M. Hammel and A. Sali, *Nucleic Acids Res.*, 2010, **38**, W540; E. F. Pettersen, T. D. Goddard, C. C. Huang, G. S. Couch, D. M. Greenblatt, E. C. Meng and T. E. Ferrin, *J. Comput. Chem.*, 2004, **25**, 1605.

blood

2012 119: 5405-5416
Prepublished online April 27, 2012;
doi:10.1182/blood-2011-11-390849

MT1-MMP plays a critical role in hematopoiesis by regulating HIF-mediated chemokine/cytokine gene transcription within niche cells

Chiemi Nishida, Kaori Kusubata, Yoshihiko Tashiro, Ismael Gritli, Aki Sato, Makiko Ohki-Koizumi, Yohei Morita, Makoto Nagano, Takeharu Sakamoto, Naohiko Koshikawa, Takahiro Kuchimaru, Shinae Kizaka-Kondoh, Motoharu Seiki, Hiromitsu Nakauchi, Beate Heissig and Koichi Hattori

Blood (print ISSN 0006-4971, online ISSN 1528-0020), is published weekly by the American Society of Hematology, 2021 L St, NW, Suite 900, Washington DC 20036.

MT1-MMP plays a critical role in hematopoiesis by regulating HIF-mediated chemokine/cytokine gene transcription within niche cells

Chiemi Nishida,[1] Kaori Kusubata,[2] Yoshihiko Tashiro,[1] Ismael Gritli,[1] Aki Sato,[1] Makiko Ohki-Koizumi,[1] Yohei Morita,[1] Makoto Nagano,[3] Takeharu Sakamoto,[3] Naohiko Koshikawa,[3] Takahiro Kuchimaru,[4] Shinae Kizaka-Kondoh,[4] Motoharu Seiki,[3] Hiromitsu Nakauchi,[1] *Beate Heissig,[1,2,5] and *Koichi Hattori[1,5]

[1]Center for Stem Cell Biology and Regenerative Medicine, Institute of Medical Science, University of Tokyo, Tokyo, Japan; [2]Frontier Research Initiative, Institute of Medical Science, University of Tokyo, Tokyo, Japan; [3]Division of Cancer Cell Research, Institute of Medical Science, University of Tokyo, Tokyo, Japan; [4]Department of Biomolecular Engineering, Tokyo Institute of Technology, Yokohama, Japan; and [5]Atopy (Allergy) Research Center, Juntendo University School of Medicine, Tokyo, Japan

HSC fate decisions are regulated by cell-intrinsic and cell-extrinsic cues. The latter cues are derived from the BM niche. Membrane-type 1 matrix metalloproteinase (MT1-MMP), which is best known for its proteolytic role in pericellular matrix remodeling, is highly expressed in HSCs and stromal/niche cells. We found that, in MT1-MMP$^{-/-}$ mice, in addition to a stem cell defect, the transcription and release of kit ligand (KitL), stromal cell–derived factor-1 (SDF-1/CXCL12), erythropoietin (Epo), and IL-7 was impaired, resulting in a trilineage hematopoietic differentiation block, while addition of exogenous KitL and SDF-1 restored hematopoiesis. Further mechanistic studies revealed that MT1-MMP activates the hypoxia-inducible factor-1 (HIF-1) pathway via factor inhibiting HIF-1 (FIH-1) within niche cells, thereby inducing the transcription of HIF-responsive genes, which induce terminal hematopoietic differentiation. Thus, MT1-MMP in niche cells regulates postnatal hematopoiesis, by modulating hematopoietic HIF-dependent niche factors that are critical for terminal differentiation and migration. (*Blood*. 2012;119(23):5405-5416)

Introduction

The adult hematopoietic system is maintained by a small number of HSCs that reside in the BM in a specialized microenvironment (the niche).[1,2] Here, HSCs undertake fate decisions including differentiation to progenitor cells and self-renewal, which ensures a lifelong supply of terminally differentiated blood cells. Intrinsic cellular programming and external stimuli such as adhesive interactions with the microenvironmental stroma and cytokine activities regulate HSC fate. However, it is unclear how niche factor production is controlled to adjust to external demand with a fine-tuned response.

Hypoxia-inducible factors (HIFs) consist of an α (HIF-α) and a β (HIF-β, or ARNT) subunit and activate the expression of genes encoding proteins that regulate cell metabolism, motility, angiogenesis, hematopoiesis, and other functions. HSCs maintain cell-cycle quiescence by regulating HIF-1α levels.[3,4] Mice with mutations in the heterodimeric transcription factor HIF develop extensive hematopoietic pathologies: embryos lacking *Arnt* have defects in primitive hematopoiesis.[5] Mice lacking endothelial PAS domain protein 1 (EPAS1, also known as HIF-2alpha/HRF/HLF/MOP3), a second HIF family member, exhibited pancytopenia, and it was shown that EPAS1 is necessary to maintain a functional microenvironment in the BM for effective hematopoiesis.[6] HIFs bind to canonical DNA sequences in the promoters or enhancers of target genes such as erythropoietin (*Epo*), vascular endothelial growth factor-A, *SDF-1α*/CXCL12, angiopoietin-2, platelet-derived growth factor-B and Kit Ligand (*KitL*)/stem cell factor, which are involved in HSC maintenance within the BM niche.[7-10] The chemokine SDF-1α/CXCL12 (SDF-1α) is expressed by perivascular, endosteal, mesenchymal stem and progenitor cells as well as by osteoblasts.[11,12] SDF-1α deficiency leads to a reduction in HSCs and impaired B-cell development in mice.[13,14] IL-7 is another stromal cell–derived niche factor, which, in cooperation with CXCL12, functions at sequential stages of B-cell development.[15,16] IL-7 or IL-7R deficiency results in impaired B-cell development.[17,18]

Proteases such as matrix metalloproteinase-9 (MMP-9) and the serine proteinase plasmin(ogen) regulate HSC fate through KitL release in the BM.[10,19] Membrane type-1 MMP (MT1-MMP, also known as MMP-14) can proteolytically degrade extracellular matrix (ECM) components and cleave membrane receptors and ligands.[20] MT1-MMP is expressed within mesenchymal stem and immature hematopoietic cells.[21,22] MT1-MMP can control the migration of hematopoietic stem/progenitor cells and monocytes.[21,23,24] MT1-MMP function is essential for angiogenesis, wound healing, connective tissue remodeling, arthritis, tumor growth, and metastasis.[25-27] MT1-MMP–deficient (MT1-MMP$^{-/-}$) mice showed skeletal dysplasia, arthritis, and osteopenia.[28] However, the role of MT1-MMP in hematopoiesis is unclear.

We found that MT1-MMP inactivation in mice resulted in severe pancytopenia, characterized by an impaired stem cell pool and a block in hematopoietic differentiation. MT1-MMP deletion from hematopoietic cells generated normal hematopoiesis in recipient mice, thereby demonstrating that MT1-MMP is an essential regulator of the BM microenvironment. Mechanistically, we demonstrate that MT1-MMP deficiency blocked the transcription of

Submitted November 8, 2011; accepted April 21, 2012. Prepublished online as *Blood* First Edition paper, April 27, 2012; DOI 10.1182/blood-2011-11-390849.

*B.H. and K.H. share senior authorship.

The online version of this article contains a data supplement.

The publication costs of this article were defrayed in part by page charge payment. Therefore, and solely to indicate this fact, this article is hereby marked "advertisement" in accordance with 18 USC section 1734.

typical HIF-1–dependent niche factors including Epo, SDF-1, KitL, and IL-7 by modulating the HIF-1 pathway through factor inhibiting HIF-1 (FIH1), resulting in a 3-lineage terminal differentiation block. Thus, MT1-MMP controls HSC fate by regulating the BM niche.

Methods

Animals

Age-matched (14-day) MT1-MMP$^{+/+}$ and MT1-MMP$^{-/-}$ mice were obtained by heterozygous breeding.[24] Animal procedures were approved by the Animal Care Committee of The Institute of Medical Science (University of Tokyo). C57BL/6 and C57BL/6-Tg (CAG-EGFP) mice were purchased from Japan SLC Inc, and Ly5.1 mice were purchased from Sankyo Lab Service.

In vivo assays

Competitive transplantation experiments. Lethally irradiated Ly-5.1 mice were injected with BM cells (10 recipient mice per cell concentration) from MT1-MMP$^{+/+}$ or MT1-MMP$^{-/-}$ mice together with 2×10^5 CD45.1 BM competitive cells. Peripheral blood (PB) cells of the recipient mice were analyzed 4 months after transplantation. Cells were stained with PE-conjugated anti-CD4 and anti-CD8, FITC-conjugated anti-CD45.2, allophycocyanin-conjugated anti-CD11b and anti-Gr-1, PE-cy7–conjugated anti-B220, and biotinylated anti-CD45.1 Abs. The biotinylated Ab was developed using streptavidin-PE–Cy5. The percentage of donor-derived lineage contributions in PBMCs was assessed using Abs against CD45.2, Gr-1/CD11b, or B220. Total chimerism of > 1% for all Abs tested using PBMCs was considered as long-term reconstitution. The frequencies were determined using L-Calc software (StemCell Technologies).

Growth factor rescue experiments. Recombinant mouse KitL (PeproTech) was administered IP into MT1-MMP$^{+/+}$ and MT1-MMP$^{-/-}$ mice at a concentration of 150 μg/kg body weight, daily from postnatal day 7 to day 10. Recombinant mouse SDF-1α (PeproTech; 100 ng/mice) was injected twice intraperitoneally on postnatal day 10. Blood was collected and blood cells counted on day 12.

CFU-S assay. Mobilized PBMCs were obtained and subjected to a CFU-S assay as previously described.[29] Mice were killed on day 12. The number of visible splenic colonies was counted.

In vitro assays

Peripheral blood analysis. Blood was collected from mice by retro-orbital bleeding using heparinized capillaries. White blood cell (WBC), RBC, and platelet (PLT) counts were determined. Plasma samples were stored at −80°C until further analysis.

Hematopoietic progenitor assay. BM mononuclear cells (BMMCs; 10^4 cells/plate) were plated in triplicate in 1 mL of a commercially available methylcellulose-based assay solution (Methocult; StemCell Technologies).

Lineage-negative cell separation. Murine BM cells were obtained after flushing mouse femur and tibiae. Cells were stained using a lineage cell separation kit (StemCell Technologies). After MACS cell separation (Miltenyi Biotec), cells were stained with c-Kit, Sca-1, and lineage Abs (BD Pharmingen), and were then analyzed by FACS.

B-cell colony-forming assay (CFU–IL-7). The CFU–IL-7 assay was carried out in medium (Invitrogen) containing 1.2% methylcellulose (StemCell Technologies), 30% FCS (HyClone), 1% BSA, 0.1mM 2-ME, and mouse IL-7 (PeproTech). On day 7 of culture, aggregates consisting of > 50 cells were scored as a colony.

Cell culture. Mouse stromal cells (MS-5) were maintained in IMDM supplemented with 10% FBS. Human BM endothelial cells (BMEC-1) were maintained in Medium 199 supplemented with 10% FBS, 0.146 mg/mL L-glutamine, and 2.2 mg/mL sodium bicarbonate. Mouse embryonic fibroblast cells (NIH3T3) were maintained in DMEM supplemented with 10% FBS. These cells were cultured at 37°C, in a 5% CO_2 incubator. Human osteoblastic cells (FOB) were maintained in a 1:1 mixture of Ham F12 medium DMEM supplemented with 2.5mM L-glutamine and 10% FBS, and the cells were cultured at 34°C, in a 5% CO_2 incubator. MT1-MMP$^{+/+}$ and MT1-MMP$^{-/-}$ mouse embryonic fibroblasts (MEF) cells (kindly provided by M.S.) were maintained in DMEM (Invitrogen) supplemented with 10% FBS at 37°C, in a 5% CO_2 incubator.[30]

Knockdown experiment using shRNA. The shRNA sequences used for knockdown of mouse MT1-MMP and FIH-1 were: 5′-caccgctgtggtgttc-cggataagtcgaaacttatccggaacaccacagc-3′ and 5′-caccggacctcgaatacctgcaagac-gaatcttgcaggtattcgaggtcctttt-3′, respectively. These sequences were subcloned into pENTR/U6 TOPO (Invitrogen) and then transferred via recombination into the lentivirus vector pLenti6 BLOCKiT (Invitrogen). shRNA-expressing lentiviral vectors were generated and used according to the manufacturer's instructions.

FACS analysis. Cells were flushed out from mouse BM. For cell-surface analysis, cells were stained with the following Abs: PE-conjugated anti-CD19, -Sca-1, -B220, CD44, c-kit, and -Gr1, FITC-conjugated anti-CD43, -CD34, -NK1.1, and -CD8, allophycocyanin-conjugated anti-B220, -CD4, CD11b, and a lineage cocktail, PerCP-Cy5.1–conjugated anti-c-kit. Cells were analyzed using FACS Aria (BD Biosciences). Common myeloid progenitor (CMP), granulocyte/macrophage progenitor (GMP), and megakaryocyte/erythroid progenitor (MEP) were determined in Lin$^-$ BM cells of 14-day-old MT1-MMP$^{+/+}$ and MT1-MMP$^{-/-}$ mice. The following Abs were used: c-kit–allophycocyanin, Sca1-PE/Cy7, CD34-FITC, FcgRIII-PE all from BD Pharmingen. For the detection of Lin$^-$ cells, biotinylated Abs (B220-bio, Gr-1-bio, CD11b-bio, CD5-bio, Ter119-bio, 7-4-bio, from Miltenyi Biotec) were costained with allophycocyanin/Cy7-conjugated (BD Biosciences/BD Pharmingen) streptavidin. For mesenchymal stem cells (MSCs) detection, cells were stained with the following Abs: CD45-PE, Sca1-FITC, PDGFRα-allophycocyanin (eBioscience), TER119-PE (BD Bioscience), CD45–Pacific Blue (BioLegend), and Alexa 488–conjugated nestin Ab (Abcam).

RNA extraction, RT-PCR, and quantitative real-time PCR analysis. Total RNA was extracted using RNA TRIzol (Invitrogen), and cDNA was generated according to the manufacturer's protocols. This cDNA (10 ng) was used as a template for each PCR amplification using the following specific forward and reverse primers, respectively: mouse *β-actin* (5′-tggaatcctgtggcatccatgaaac-3′) and (5′-taaaacgcagctcagtaacagtccg-3′); mouse *MT1-MMP* (5′-tccggataagtttgggactg-3′) and (5′-ccttcaccatcaaagggtgt-3′); human *GAPDH* (5′-gagtcaacggatttggtcgt-3′) and (5′-ttgattttggagggatctcg-3′); human *MT1-MMP* (5′-caagcattgggtgtttgatgatg-3′) and (5′-cttggggg-tactcgctatcca-3′). For quantitative real-time PCR, PCR mixtures were prepared using SYBR Premix Ex TaqII (Takara) containing 0.2mM of each primer, and amplification reactions were performed. Specific forward and reverse primers, respectively, were designed as follows: *β-actin* (5′-gctggaaggtggacagtgag-3′) and (5′-tgacaggatgcagaaggaga-3′); *KitL* (5′-gcctagtcattgttggctac-3′) and (5′-cccaagtttgtctatgatgg-3′); *SDF-1* (5′-agaaaccttccaccagagca-3′) and (5′-aacggctaggaaagggtctc-3′); *IL-7* (5′-tgcaatcatgtcaactgcaa-3′) and (5′-tgcaatcatgtcaactgcaa-3′); *EPO* (5′-catctgcgacagtcgagttctg-3′) and (5′-cacaacccatcgtgacattttc-3′); *G-CSF* (5′-cctgcttagagcagagagag-3′) and (5′-cagcagcaggaatcaatact-3′). Gene expression levels were measured using the ABI Prism 7500 sequence detection system (Applied Biosystems). PCR product levels were estimated by measurement of the intensity of SYBR Green fluorescence. Gene expression levels were normalized to *β-actin* mRNA.

Knockdown experiment using siRNA. Target sequences for siRNA were commercially designed and synthesized (B-bridge). siRNAs were provided as a mixture containing 3 different siRNA target sequences. The RNAi transfection solution was prepared by preincubating a mixture of 5nM siRNAs dissolved in 1 mL of serum-free and antibiotic-free medium (OptiMEM; Invitrogen) and 10 μL of RNAiMAX for 20 minutes at room temperature. Cells (3-4.5 × 10^5 cell/4 mL growth medium without antibiotics) suspended by trypsinization were added to the mixture and cultured overnight, and the medium was replaced with fresh growth medium.

Overexpression of MT1-MMP. The transfection solution was prepared by preincubating a mixture of 1 μg of plasmid DNA dissolved in 250 μL of OptiMEM and 3 μL of Lipofectamine 2000 (Invitrogen) dissolved in 250 μL of OptiMEM for 20 minutes at room temperature. The transfection mixture (500 μL in total) was then added to the cells. After

48 hours of culture, the culture media were replaced with fresh growth medium.

Immunoprecipitation. Cells were lysed with cell lysis buffer (Cell Signaling Technology) and the supernatants were collected. Total protein content was measured using the Bradford assay (Bio-Rad). Lysates were incubated with protein-G–Sepharose beads (Santa Cruz Biotechnology) and anti–HIF-1α Ab (BD Biosciences) overnight and were then spun down for 1 minute at 5800*g*. The supernatant was removed and the pellets were solubilized with 6 × SDS sample buffer (0.35M Tris-HCl, pH 6.8, 10% SDS, 30% glycerol, 9.3% DTT) and analyzed by immunoblot analysis.

Immunoblotting. Cells were lysed with lysis buffer (Cell Signaling Technology) according to the manufacturer's instructions. The supernatants were collected, and total protein content was measured using the Bradford assay (Bio-Rad). The subcellular proteome extraction kit (Merck) was used to fractionate subcellular proteins. Lysates were separated by SDS-PAGE, transferred to a PVDF membrane, subjected to immunoblotting using anti–FIH-1 (1:200; Santa Cruz Biotechnology), anti-integrinβ1 (1/1000; Chemicon), and anti-α/β tubulin (1:1000; Cell Signaling Technology), washed with TBS-T, and immunoprobed for 1 hour at room temperature with HRP-conjugated or alkaline phosphatase–conjugated Ab, then washed with PBS-T. Finally, membranes were incubated with ECL-Plus (Amersham), and the chemiluminescent signal was detected using LAS4000 (Fujifilm) according to the manufacturer's instructions. The alkaline phosphatase signal was then detected using the Histofine Kit (Nichirei).

Immunoassay. After cell transfection with siRNA, the growth medium was replaced and the cells were cultured for 48 hours. Supernatants were then collected and analyzed for murine KitL, SDF-1α, and IL-7 using commercially available ELISAs (R&D Systems).

Stromal-based expansion cultures. A total of 1×10^4 Lin^- cells from the BM of GFP mice were cocultured with a confluent layer of stromal cells (MS-5). Recombinant mouse KitL (20 ng/mL, every other day) or recombinant mouse SDF-1α (100 ng/mL, every other day) was added to MT1-MMP KD MS-5 and control MS-5 cell cultures. Twelve days later, adherent cells were retrieved using trypsin (Sigma-Aldrich) and pooled with the nonadherent cells. Hematopoietic cells (GFP positive) were counted.

Migration assay. Migration assays were performed in 24-well plates using 5-μm polycarbonate Transwell inserts (Costar). BM Lin^- cells were collected and isolated from normal adult mice. The cells were resuspended in X-vivo 15 (Lonza). MT1-$MMP^{+/+}$ and MT1-$MMP^{-/-}$ MEF culture supernatant was aliquoted (600-μL aliquots) into 24-well plates, which formed the bottom chamber, in the presence or absence of neutralizing Abs against mouse SDF-1 (R&D Systems). Lin^- cells derived from the BM cells of GFP mice (2×10^5 cells in 100 μL) were added into the Transwell insert (top chamber), and the cells were allowed to migrate through the porous bottom for 4 hours at 37°C. The number of cells that migrated into the lower chamber was determined using flow cytometry. Cells had been stained with Abs against CD11b and Gr1 (BD Biosciences). The medium from the lower chamber was passed through a FACSCalibur for 60 seconds, gating on forward (FSC) and side scatter to exclude cell debris. The number of live cells was compared with a 100% migration control in which 2×10^5 cells had been added directly into the lower chamber and then counted on the FACScalibur for 60 seconds.

Immunohistochemistry. BM sections were fixed with 4% paraformaldehyde and permeabilized using 0.2% Triton X-100 for 20 minutes. After blocking in PBS containing 5% goat serum and 0.2% BSA, the sections were incubated with anti–FIH-1 Ab (Novus Biologicals) for 16 hours, washed 3 times with PBS and incubated for 1 hour with anti–rabbit Alexa 568 (Invitrogen). After washing, the sections were incubated with Alexa 488–conjugated nestin Ab (Abcam) for 2 hours. For HIF-1 staining, fixed and blocked sections were incubated with Alexa 488–conjugated HIF-1 Ab (BD Pharmingen) for 2 hours. The sections were mounted using Vectashield Mounting Medium with DAPI (Vector Laboratories). Images were acquired with an Olympus DP71 camera.

Micro-CT analysis. We evaluated the BM shaft surface area by using micro-CT (Rigaku). We measured the shaft area at the center of the femur by NIH ImageJ software.

Proliferation assay. A total of 2×10^4 Lin^- cells isolated by MACS (Miltenyi Biotec) from BM cells of GFP mice were cocultured with a confluent layer of MEF cells. The cells were maintained in X-vivo 15 supplemented recombinant mouse IL-3 (20 ng/mL, every other day) with or without neutralizing Abs against mouse KitL (R&D Systems). One week later, all cells were retrieved using trypsin (Sigma-Aldrich). GFP-positive were counted using FACS.

Statistical analysis

Data were analyzed using the unpaired 2-tailed Student *t* test and are expressed as means ± SEM. *P* values of $< .05$ were considered significant.

Results

MT1-MMP deletion leads to severe pancytopenia

We used 14-day-old MT1-$MMP^{-/-}$ mice to explore the role of MT1-MMP in the regulation of postnatal hematopoiesis, as mortality of older MT1-$MMP^{-/-}$ mice is very high.[24,28] Compared with MT1-$MMP^{+/+}$ mice, the body weight of MT1-$MMP^{-/-}$ mice was decreased (7.22 ± 0.48 and 2.99 ± 0.05 g/mouse, respectively; n = 5, $P < .001$) and there was a decline in all hematopoietic lineages examined in MT1-$MMP^{-/-}$ animals, including WBCs (Figure 1A), PLTs (Figure 1B), and RBCs (Figure 1C) in the PB. MT1-$MMP^{-/-}$ hematopoietic femurs were smaller than MT1-$MMP^{+/+}$ femurs (Figure 1D). Under steady-state conditions, BM cellularity in MT1-MMP mice was decreased compared with MT1-$MMP^{+/+}$ mice (Figure 1E). We next analyzed the number of MSCs by flow cytometry. The frequency of $PDGFR\alpha^+/Sca1^+/CD45^-/Ter119^-$ BM-derived MSCs and $nestin^+$ niche cells was lower in MT1-$MMP^{-/-}$ BM cells than in MT1-$MMP^{+/+}$ BM cells (Figure 1F).[31] Because the skeletal malformation described in MT1-$MMP^{-/-}$ mice could affect the intrafemural space where hematopoiesis occurs, the BM shaft surface area was determined by microcomputer tomography (microCT). The BM shaft surface area was reduced in MT1-$MMP^{-/-}$ femurs compared with MT1-$MMP^{+/+}$ mice (Figure 1G).

Histologic analysis of BM sections showed that MT1-$MMP^{-/-}$ mice exhibited a striking paucity of hematopoietic cells within the BM shaft and a reduction in the number of megakaryocytes, which are responsible for platelet production (Figure 1H-I).

We next examined HSCs and hematopoietic progenitor populations. In wild-type mice, MT1-MMP is expressed in primary BMMCs within the lineage-negative (Lin^-) cell fraction, which contains mostly hematopoietic progenitor cells and a small fraction of HSCs, and in BM stromal cells, including BM endothelial cells (BMEC-1), fetal osteoblasts (FOB), and fibroblast-like stromal cells (MS-5; Figure 1J-K). The absolute number of CFU cells (CFU-C; Figure 1L) and of more primitive progenitor populations within BM cells, including day-8 CFU-spleen (CFU-S; Figure 1M), CMPs, GMPs, and MEPs and HSC-enriched $CD34^-c\text{-}Kit^+$, $Sca\text{-}1^+$, Lin^- (KSL) cells were diminished in MT1-$MMP^{-/-}$ BMMCs. To determine the HSC content of the BM, we performed limiting-dilution competitive repopulation analysis using MT1-$MMP^{+/+}$ or MT1-$MMP^{-/-}$ BMMCs. There was a lower frequency, and a significantly reduced absolute number of competitive repopulation units (CRUs) per femur in MT1-$MMP^{-/-}$ BMMCs than in MT1-$MMP^{+/+}$ BMMCs. These data indicate that MT1-MMP is required for HSC maintenance and for normal hematopoietic differentiation.

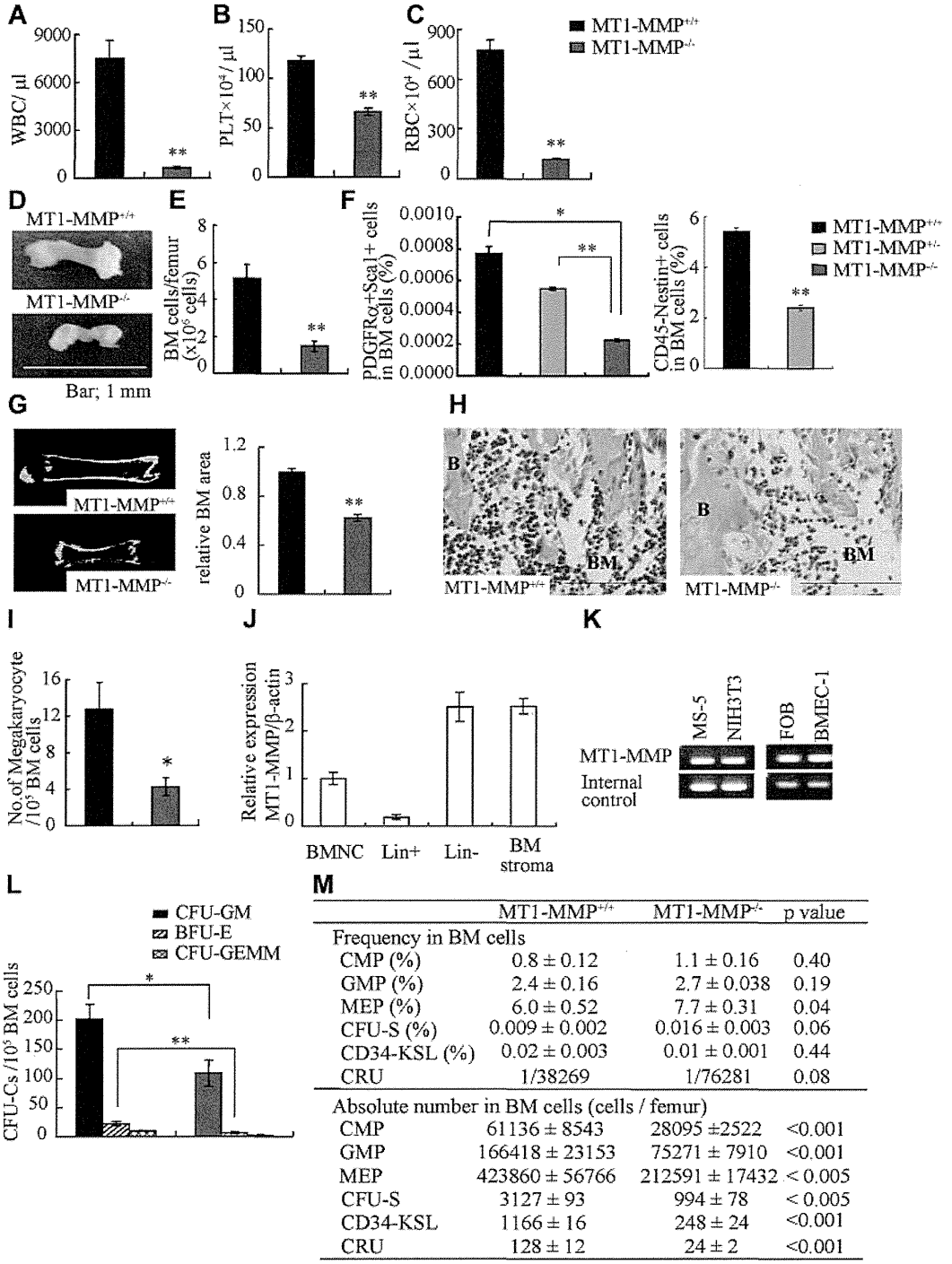

M

	MT1-MMP$^{+/+}$	MT1-MMP$^{-/-}$	p value
Frequency in BM cells			
CMP (%)	0.8 ± 0.12	1.1 ± 0.16	0.40
GMP (%)	2.4 ± 0.16	2.7 ± 0.038	0.19
MEP (%)	6.0 ± 0.52	7.7 ± 0.31	0.04
CFU-S (%)	0.009 ± 0.002	0.016 ± 0.003	0.06
CD34-KSL (%)	0.02 ± 0.003	0.01 ± 0.001	0.44
CRU	1/38269	1/76281	0.08
Absolute number in BM cells (cells / femur)			
CMP	61136 ± 8543	28095 ±2522	<0.001
GMP	166418 ± 23153	75271 ± 7910	<0.001
MEP	423860 ± 56766	212591 ± 17432	< 0.005
CFU-S	3127 ± 93	994 ± 78	< 0.005
CD34-KSL	1166 ± 16	248 ± 24	<0.001
CRU	128 ± 12	24 ± 2	<0.001

Figure 1. MT1-MMP gene deletion causes myelosuppression. (A-C) The number of (A) WBCs, (B) platelets (PLT), and (C) RBCs in the PB of 14-day-old mice was counted (n = 8). (D) Images of mouse femurs (bars, 1 mm). (E) Total BM cell number per femur. (F) The percentage of PDGFRα$^+$Sca1$^+$ cells (MSCs) was determined by flow cytometry (n = 2). (G) (left panel) Representative MicroCT scan images, and (right panel) quantification of the relative BM area within the BM femur shaft are presented (n = 3). (H) H&E-stained femur sections. Right panel shows the quantification of the BM area per femur. B indicates bone, (bars, 200 μm). (I) Megakaryocyte number (n = 5). (J-K) Real-time PCR analysis of MT1-MMP expression in (J) BM nuclear cells (BMNCs), Lin$^+$, Lin$^-$, and BM stroma cells, and (K) in MS-5, NIH3T3, FOB, and BMEC-1 cells. (L-M) The (L) absolute number of CFU-C per 10^5 BM cells and (M) frequency and absolute number/femur of CFU-S, CMP, GMP, MEP, CD34-KSL cells, and competitive repopulating units (CRU) in wild-type and knockout BM cells (n = 3). For CRU determination, freshly isolated BM cells of different cell concentration were transplanted into recipients (n = 10). Four months posttransplantation, the repopulating unit (RU) with trilineage engraftment (> 1% of donor-derived cells) was calculated. The absolute number of CRU was calculated based on the observed number of BM cells per femur. Errors in bar graphs are SEM; $^*P < .05$, $^{**}P < .01$. CFU-C indicates CFU cells; CFU-S, CFU-spleen; CMP, common myeloid progenitor; GMP, granulocyte/macrophage lineage-restricted progenitor; and MEP, megakaryocyte/erythrocyte lineage-restricted progenitor.

MT1-MMP$^{-/-}$ mice show a T- and B-cell differentiation defect

Compared with MT1-MMP$^{+/+}$ mice, the absolute numbers of PB CD3$^+$ T and B220$^+$ B lymphocytes were reduced (Figure 2A) and the spleen was much smaller (Figure 2B) in MT1-MMP$^{-/-}$ mice. Similar to the BM, histologic examination revealed less megakaryocytes in the MT1-MMP$^{-/-}$ spleen (Figure 2C). The white pulp appeared smaller in MT1-MMP$^{-/-}$ spleens (Figure 2C), which correlated with a reduction in the absolute numbers of lymphoid

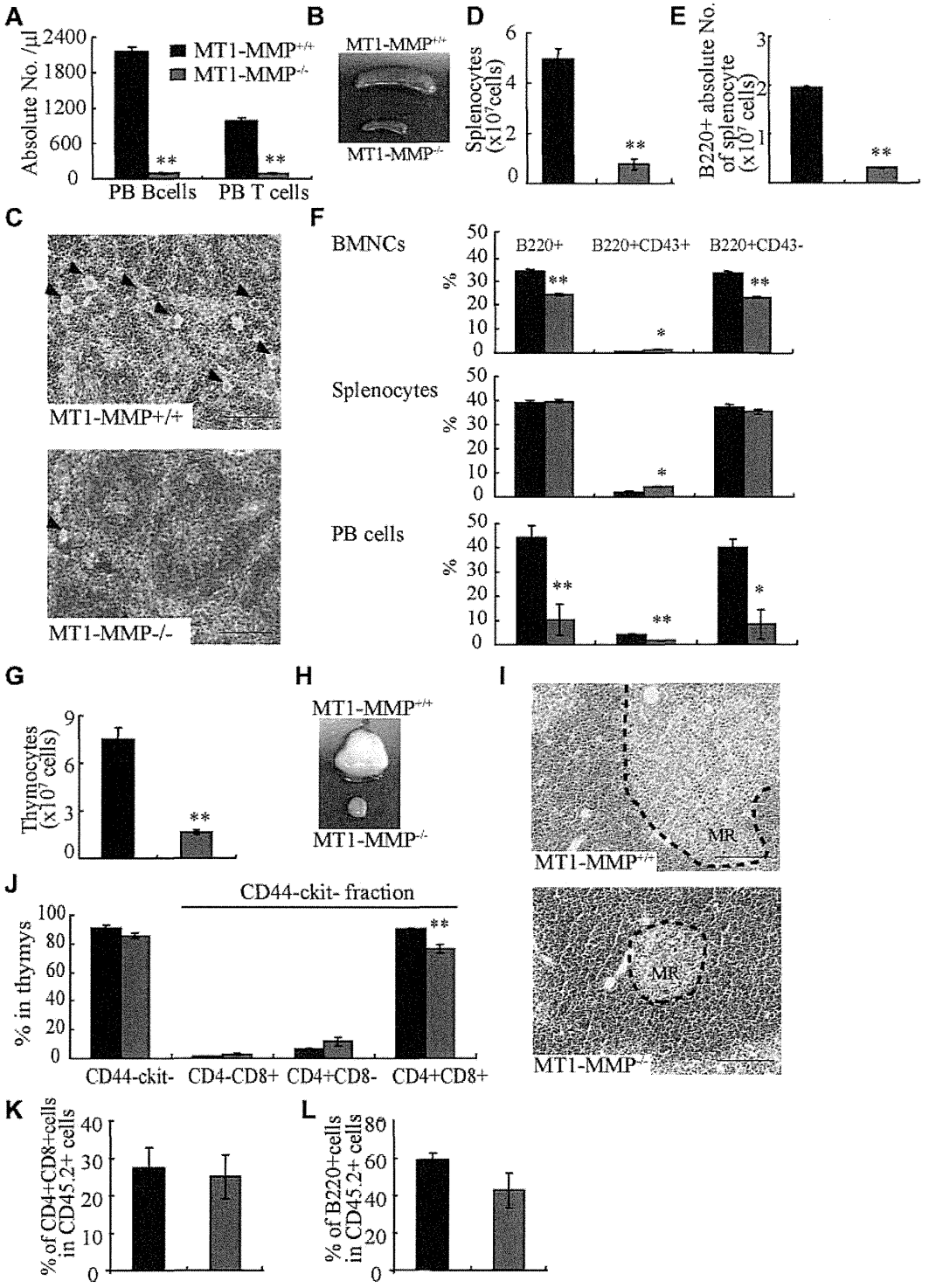

Figure 2. T and B lymphopoiesis are impaired in MT1-MMP$^{-/-}$ mice. (A) PB B- and T-cell numbers (FACS analysis). (B) Images of mouse spleens. (C) H&E-stained spleen sections. Arrowheads indicate megakaryocytes (bars, 100 μm). (D-E) The (D) total number of splenocytes and (E) B220$^+$ cells in splenocytes (n ≥ 6). (F) The percentage of B220$^+$ populations in BMNCs (n = 6), splenocytes (n = 3), and PB cells (n = 2). (G) Thymocyte number (n = 4). (H) Images of thymi. (I) H&E-stained thymus sections. MR indicates medullar region (bars, 100 μm). (J) The percentage of thymic T-lineage subpopulations. (K-L) BM cells from MT1-MMP$^{+/+}$ and MT1-MMP$^{-/-}$ mice were transplanted into wild-type animals (CD45.2). (K) The percentage of donor CD4$^+$/CD8$^+$ T and (L) B220$^+$B cell lineage contribution of donor-derived cells in the PB 4 months after transplantation (n = 10/group). Errors in bar graphs are SEM; *$P < .05$, **$P < .01$.

and total B (B220$^+$) spleen cells (Figure 2D-E). The percentage of B220$^+$, early- (B220$^+$CD43$^+$), and late-stage (B220$^+$CD43$^-$) B cells was reduced in MT1-MMP$^{-/-}$ BM, spleen, and PBMCs (Figure 2F). Although the absolute number of early- and late-stage B cells in splenocytes was reduced in MT1-MMP$^{-/-}$ mice (data not shown), the relative percentage of early (B220$^+$CD43$^+$) B cells was augmented in MT1-MMP$^{-/-}$ splenocytes. These data demonstrate that MT1-MMP is required for normal terminal B-cell differentiation within the BM with impaired release of B cells into the circulation.

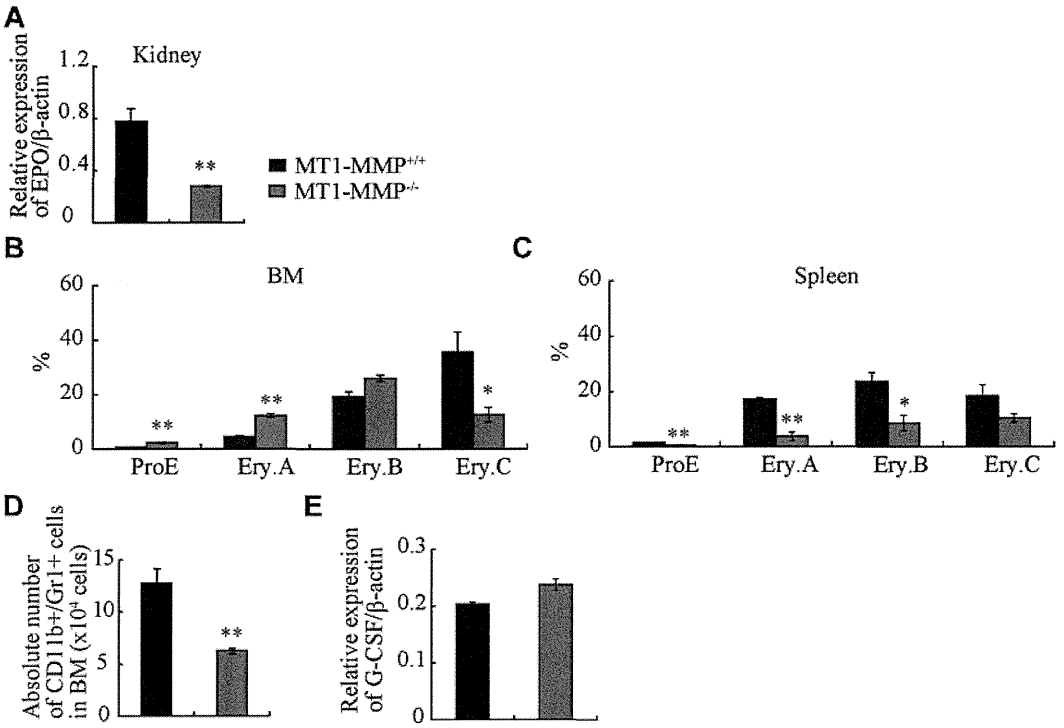

Figure 3. Erythroid and myeloid differentiation block in MT1-MMP$^{-/-}$ mice. (A) Real-time PCR of *Epo* in kidney (n = 3). (B-C) Percentage of different erythroblast populations during erythroid development (proE-EryA-EryB-EryC) of (B) BM cells or of (C) dissociated mouse spleen cells from MT1-MMP$^{+/+}$ (n = 5) and MT1-MMP$^{-/-}$ mice (n = 3). (D) Percentage of CD11b^{+}/Gr-1^{+} cells per femur as determined by FACS (n = 5). Errors in bar graphs are SEM; $^{**}P < .01$. (E) Real-time PCR of *G-CSF* in BM cells (n = 3).

The earliest T-cell progenitors are produced in the BM. We found an increase in the percentage of immature CD4^{-}CD8^{-}c-Kit^{-}CD44^{-} cells T cells in MT1-MMP$^{-/-}$ BM cells ($4.1 \times 10^5 \pm 0.2 \times 10^5$ cells in MT1-MMP$^{-/-}$ and $2.6 \times 10^5 \pm 0.3 \times 10^5$ cells in MT1-MMP$^{+/+}$ BM, respectively; n = 4, $P < .05$). The MT1-MMP$^{-/-}$ thymus (Figure 2G) was small with a low number of thymocytes (Figure 2H). Thymic lobes, and specifically the medullar region, appeared smaller than in MT1-MMP$^{+/+}$ mice (Figure 2I). Flow cytometric analysis of thymocytes revealed no difference in the percentage of immature CD4^{-} or CD8^{-} double-negative (DN) thymocytes or of CD4^{-}CD8^{-}c-Kit^{-}CD44^{-} thymocytes between the MT1-MMP$^{+/+}$ and the MT1-MMP$^{-/-}$ mice. However, a relative decrease in the percentage of the more mature CD4^{+}CD8^{+} double-positive (DP) thymocyte population and in the CD4^{+} single-positive (SP) cell population was revealed in thymocytes from the MT1-MMP$^{-/-}$ mice (Figure 2J). In absolute terms, CD4 SP numbers were reduced 2.5-fold, CD8 SP 2.1-fold, and DP thymocytes 5.3-fold, whereas the DN population remained unaffected. These data indicate that T-cell progenitors developed within the BM even in the absence of MT1-MMP, but that their further differentiation in the thymus was blocked at or before development of the immature DN thymocyte population, causing default differentiation into CD4 cell SP and NK-cell lineages.

To assess whether the abnormal thymic colonization observed in MT1-MMP$^{-/-}$ mice was because of the loss of MT1-MMP in hematopoietic cells or in stromal cells, MT1-MMP$^{+/+}$ and MT1-MMP$^{-/-}$ BM donor cells were transplanted into lethally irradiated wild-type recipients. Chimeras were analyzed 4 months after transplantation. T- and B-cell differentiation of transplanted MT1-MMP$^{-/-}$ cells (expressing the Ag Ly5.2 (CD45.2) on leukocytes) within the BM were normal (Figure 2K-L). These data indicated that MT1-MMP$^{-/-}$ mice showed impaired T- and B-cell development. Even though MT1-MMP$^{-/-}$ mice showed a hematopoietic cell defect (see Figure 1), MT1-MMP$^{-/-}$ BM cells retained the potential to differentiate into T- and B-cell lineages in an MT1-MMP$^{+/+}$ environment. These data indicate that, aside from its influence on stem cells, MT1-MMP also plays an additional role in regulating the BM niche.

MT1-MMP ablation impairs erythroid and myeloid differentiation

Anemia, as seen in 14-day-old MT1-MMP mice (see Figure 1C), is expected to trigger a compensatory response that is mediated principally through increased serum levels of erythropoietin (*Epo*), a master cytokine of erythropoiesis. Epo controls growth, survival, and differentiation of erythroid progenitors, either cooperatively with, or independently of KitL.[32-34] Despite severe anemia, *Epo* mRNA expression in kidney tissues of MT1-MMP$^{-/-}$ mice was low (Figure 3A) and the expected compensatory increase in spleen size did not occur (see Figure 2B).

To assess erythroid differentiation, we examined CD71 and TER119 expression in the BM and splenic erythroblasts, and classified erythroid cells into 4 populations at progressive levels of differentiation: proerythroblasts TER119^{med}CD71^{high}FSC^{high} (ProE), TER119^{high}CD71^{high}FSC^{high} (Ery.A), TER119^{high}CD71^{high}FSC^{low} (Ery.B), and TER119^{high}CD71^{low}FSC^{low} (Ery.C).[35]

MT1-MMP$^{-/-}$ BM erythroid lineage cells accumulated at the ProE, Ery.A, and Ery.B stage, and cells at the late erythroblast differentiation stages (Ery.C) were reduced (Figure 3B). In spleen, all stages of erythroid lineage cells were reduced in MT1-MMP$^{-/-}$ mice (Figure 3C). These data suggest that MT1-MMP is involved in both BM and splenic erythropoiesis, and that the defect in erythropoiesis in MT1-MMP$^{-/-}$ mice might be due, in part, to impaired Epo production.